Functional design of tentacles in squid: linking sarcomere ultrastructure to gross morphological dynamics

J. L. VAN LEEUWEN[1,2] AND W. M. KIER[3]

[1]*Department of Physiology, Leiden University, Wassenaarseweg 62, PO Box 9604, NL-2300 RC Leiden, The Netherlands* (`j.l.van_leeuwen@physiology.medfac.leidenuniv.nl`)
[2]*Institute for Sport Science, LSB Biomechanics, Friedrich Schiller University, Seidelstraße 20, D-07749 Jena, Germany*
[3]*Department of Biology, CB#3280 Coker Hall, University of North Carolina, Chapel Hill, NC 27599-3280, USA*

CONTENTS

SUMMARY

This paper offers a quantitative analysis of tentacle extension in squid that integrates several levels of structural organization. The muscular stalks of the two tentacles of squid are rapidly elongated by 70% of resting length during prey capture. A typical duration of the extension is 30 ms in *Loligo pealei* (with a contracted tentacle length of 93 mm and a strike distance of about 37 mm). In a successful strike, the terminal clubs hit the prey and attach to it via arrays of suckers.

A forward dynamics model is proposed for the extension of the tentacular stalk and the forward motion of the terminal club. The stalk is modelled as a longitudinal array of thin muscular discs with extensor muscle fibres oriented parallel to the disc planes. As a disc contracts radially, it lengthens because its volume is constant. The equations of motion for the linked system of discs were formulated and solved numerically. The inputs of the model are the dimensions of the tentacle, passive and active muscle properties such as Hill's force–velocity relationship, myofilament lengths and activation of the muscle fibres. The model predicts the changing geometry of the tentacle, the pressure and stress distribution inside the tentacle and the velocity and kinetic energy distribution of the stalk and club. These predictions are in agreement with kinematic observations from high-speed films of prey capture. The model demonstrates also that the unusually short myosin filaments (reported range 0.5–0.9 µm) that characterize the extensor muscles are necessary for the observed extension performance. Myosin filament lengths typical for vertebrate sarcomeres (1.58 µm) would lead to a significant reduction in performance. In addition, the model predicts that, to maximize peak velocity of the terminal club, the myosin filaments should be longer at the base and shorter at the tip of the stalk (0.97 µm at the base and 0.50 µm at the tip for the tentacle size above). This results from differences in dynamic loading along the stalk. Finally, the model allows exploration of the effects of changes in the dimensions and mass of the tentacle and intrinsic speed of the myofilaments on the optimum myosin filament lengths.

1. INTRODUCTION

Squid and cuttlefish have two tentacles and eight arms which are used to capture and to manipulate prey. These appendages are muscular hydrostats, muscular organs that lack hard skeletal support. Activation of the muscle fibres may cause large deformations, which are generally difficult to predict and to analyse because of the biphasic fibre–fluid nature of the tissue and the nonlinear properties of the mus-

cle fibres and connective tissue elements. During prey capture, the squid swims forward, flares its arms outwards and backwards, and elongates its tentacles (see figure 1a and Kier (1982) for a qualitative description). Similar behaviour is displayed by the cuttlefish *Sepia officinalis* (Messenger 1968, 1977).

The tentacular morphology of cephalopods was described by Guérin (1908), Williams (1909) and recently by Kier (1982). The tentacle consists of a muscular stalk and a terminal club equipped with arrays of suckers used to grasp the prey. Figure 1b shows a diagram of the muscle–fibre arrangement in the tentacular stalk of *Loligo pealei*. Obliquely striated muscle fibres are arranged longitudinally in the stalk (Kier 1985, 1991), both in a superficial layer (SLM) and in deeper bundles (LM). Similar fibres are found in helical paths (HM), running either clockwise or anticlockwise in two layers underneath the SLM layer. The helical fibres can exert a torsional moment about the stalk. They may also act as extensors or retractors, depending on the variable angle of pitch (i.e. angle with the longitudinal direction) during the strike (Kier & Smith 1985). This last possibility has yet to be investigated quantitatively. The longitudinal muscle fibres not only tend to shorten the tentacle, but may also induce bending moments along the tentacle. The extensor muscles are arranged in a layer of circularly directed fibres as well as a transversely oriented fibre group. Together they enclose the columns of longitudinal fibres.

Electron microscopic observations have revealed that the extensor muscles have sarcomeres typical of cross-striated muscles (Kier 1985, 1991). The myosin filaments, however, were found to be remarkably variable in length (range of 0.5–0.9 μm), and on average they are very short compared to those found in vertebrates (approximately 1.58 μm (Offer 1987)). Short thick filaments and sarcomeres are characteristic of fibres reaching high strain rates at the cost of a relatively low tensile stress (e.g. Josephson 1975; Van Leeuwen 1991, 1992).

A recent kinematic analysis of tentacle extension (Kier & Van Leeuwen 1997) has shown that in *Loligo pealei* a longitudinal strain (see § 4 c) of the tentacular stalk of about 0.7 can occur in 30 ms. The highest longitudinal strain rate that was observed was about $45\,\mathrm{s}^{-1}$. In the modelling section, we will show how, from this strain rate, the (negative) peak strain rate of the extensor muscles can be estimated (equation (25)).

In this paper, we discuss a forward dynamics model of the tentacle. The model includes salient geometrical aspects such as muscle–fibre arrangements and sarcomere dimensions, and widely accepted physiological properties of cross-striated muscles such as force–velocity characteristics. In the forward dynamics method, movements of body parts are calculated from a prescribed mechanical stress distribution. In studies of muscle dynamics, it is actually preferable to go one step further and calculate the stress distribution and movements starting from prescribed muscle activations (Van Leeuwen 1992). The present model accepts the active state of the muscle fibres as

input and it predicts the internal pressure and stress distribution of the stalk, the extension of the tentacle and the acceleration of the terminal club.

The most proximal parts of the tentacle experience presumably the highest dynamic loads, because these parts have the greatest tentacle mass in front of them to be pushed forward. Differences in load might be balanced by an appropriate tapering of the stalk. The tapering of the stalk along its length is, however, very limited. It may even taper very slightly from tip to base. We suggest that the higher proximal load could be withstood by increasing the myosin-filament length from the tip of the stalk to its base, because the maximum active component of muscle stress is roughly proportional to the myosin filament length. We furthermore expect that it would be favourable to adjust sarcomere lengths so as to optimize locally the work output during the very short extension time. The present model is designed to address these issues and therefore to improve the understanding of the relationships between gross morphological dynamics and various design features of the sarcomeres.

2. SYMBOLS AND DEFINITIONS

symbol	definition	unit in text
$\boldsymbol{a}$	acceleration vector with components $a_1, a_2, \ldots, a_{n-2}, a_{n-1}$	$\mathrm{m\,s^{-2}}$
a_i	acceleration in longitudinal direction of boundary b_i	$\mathrm{m\,s^{-2}}$
$a_{\max}$	maximum forward acceleration of the terminal club	$\mathrm{m\,s^{-2}}$
A_{c0}	cross-sectional area of stalk in initial state	$\mathrm{mm^2}$
$A_{c,i}$	cross-sectional area of disc i	$\mathrm{mm^2}$
A_{cl0}	cross-sectional area of longitudinal muscles in initial state	$\mathrm{mm^2}$
$A_{s0,i}$	lateral surface area of disc i in initial state	$\mathrm{mm^2}$
$A_{s,i}$	lateral surface area of disc i	$\mathrm{mm^2}$
b_i	boundary between disc i and disc $i+1$	
c_{1pas}	constant in equation (17)	kPa
c_{2pas}	constant in equation (17)	
c_{3pas}	constant in equation (17)	kPa
c_{4pas}	constant in equation (17)	kPa
C_{myo}	resistive constant for myosin filament	
$c_{x,i}$	component in equation (45), $x \in [1, 2, 3, 4]$; $i \in [1, 2, \ldots, n-2, n-1]$	varies with x
D_{act}	constant to account for cross-bridge losses due to actin filament overlap in one sarcomere	
D_{myo}	constant to account for cross-bridge losses due to interaction between myosin filament and Z-disc	
E_{kclub}	kinetic energy of tentacular club	mJ
E_{kmax}	peak kinetic energy of tentacular club	mJ
$E_{k,i}$	kinetic energy of segment i	mJ

$E_{\mathrm{kl},i}$	part of $E_{k,i}$ associated with velocity in longitudinal direction	mJ
$E_{\mathrm{kr},i}$	part of $E_{k,i}$ associated with velocity in radial direction	mJ
F_i	net force on $m_{b,i}$ by segment i	N
$f_{\mathrm{a},i}$	active state of muscle fibres in disc i	
$f_{\mathrm{l},i}$	filamentary overlap function of disc i	
$f_{\mathrm{v},i}$	velocity dependence function of disc i	
$g_{x,i}$	expression derived in the appendix, $x \in [1,2,3,4]$; $i \in [1,2,\ldots,n-2,n-1]$	varies with x
$h_{0,i}$	initial length (height) of tentacular disc i	mm
h_i	length (height) of tentacular disc i	mm
k	constant in equations (7) and (7)	
l	co-ordinate in longitudinal direction	mm
$\boldsymbol{l}$	position vector with components $l_1, l_2, \ldots, l_{n-2}, l_{n-1}$	mm
$l_{0\mathrm{sarc},i}$	optimum sarcomere length for active force production in segment i	μm
$l_{0\mathrm{sarc,ref}}$	idem, but for reference sarcomere	μm
$l_{\mathrm{act},i}$	length of two opposite thin filaments in one sarcomere of segment i	μm
l_i	position in longitudinal direction of boundary b_i	mm
l_{bz}	length of bare zone on myosin filament	μm
$l_{\mathrm{mopt},i}$	optimum length of myosin filament in segment i	μm
$l_{\mathrm{myo},i}$	length of myosin filament in segment i	μm
$l_{\mathrm{myo,ref}}$	length of myosin filament of reference sarcomere	μm
l_{s}	length of tentacular stalk	mm
l_{s0}	initial length of tentacular stalk	mm
$l_{\mathrm{sarc},i}$	sarcomere length in segment i	μm
l_{z}	width of Z-disc (kept constant along stalk)	μm
$m_{b,i}$	mass associated with boundary b_i	g
m_{club}	mass of tentacular club	g
m_l	mass per unit length along the tentacle	g mm^{-1}
n	number of segments of tentacle model	
p_i	pressure in segment i	kPa
q	exponent in activation equation (4)	
r	co-ordinate in radial direction	mm
r_i	radius of tentacular disc i	mm
r_0	initial radius of tentacular stalk	mm
t	time	ms
t_{a}	time between start of activation and first moment of full activation	ms
$t_{\mathrm{d},i}$	delay of activation of segment i with respect to segment 1	ms
u	velocity of tentacular tissue in longitudinal direction	m s^{-1}

$\boldsymbol{u}$	velocity vector with components $u_1, u_2, \ldots, u_{n-2}, u_{n-1}$	m s^{-1}
u_i	velocity in longitudinal direction of boundary b_i	m s^{-1}
u_{max}	maximum forward velocity of the terminal club	m s^{-1}
V_i	volume of disc i	mm^3
α	constant for defining the added mass of water	
ε_{c}	critical strain in equations (17) and (17)	
$\varepsilon_{\mathrm{l},i}$	strain in longitudinal direction of disc i	
$\varepsilon_{\mathrm{lmax}}$	maximum average strain of the stalk in the longitudinal direction	
$\varepsilon_{\mathrm{lstalk}}$	average strain of the stalk in the longitudinal direction	
$\varepsilon_{\mathrm{r},i}$	strain in radial direction of disc i	
$\varepsilon_{\mathrm{rmin}}$	minimum average strain in radial direction of stalk	
$\dot{\varepsilon}_{\mathrm{min},i}$	minimum unloaded strain rate of disc i	s^{-1}
$\dot{\varepsilon}_{\mathrm{min,ref}}$	minimum unloaded strain rate of reference sarcomere	s^{-1}
η	constant to correct for partial filling of stalk with extensor muscles	
μ	viscous friction parameter associated with longitudinal strain rate	g mm^{-1} s^{-1}
ν	kinematic viscosity of water around tentacle	mm^2 s^{-1}
ρ	density of tentacular tissue	kg m^{-3}
$\sigma_{\mathrm{l},i}$	average stress in longitudinal direction	kPa
$\sigma_{\mathrm{max},i}$	maximum isometric muscle stress in radial direction at $l_{0\mathrm{sarc},i}$	kPa
$\sigma_{\mathrm{max,ref}}$	maximum isometric muscle stress of reference sarcomere at $l_{0\mathrm{sarc,ref}}$	kPa
$\sigma_{\mathrm{pas},i}$	passive component of muscle stress in radial direction	kPa
$\sigma_{\mathrm{r},i}$	muscle stress in radial direction	kPa

3. MATERIALS

Specimens of the squid *Loligo pealei* (LeSueur 1821) were maintained in tanks at 19 °C as described by Kier & Van Leeuwen (1997). High-speed films were made of squid capturing shrimps. Landmarks on the body and tentacle were digitized so as to obtain position coordinates of forward body motion and tentacle extension (Kier & Van Leeuwen 1997). The digitized coordinates were smoothed and differentiated using quintic splines in combination with the criterion of generalized cross validation (Woltring 1986). Results of the kinematic analysis were used to test the dynamic model predictions (see § 6).

4. MODEL DESCRIPTION

The symbols used in this section are listed in § 2. For convenience, we will use the Newtonian notation for time derivatives.
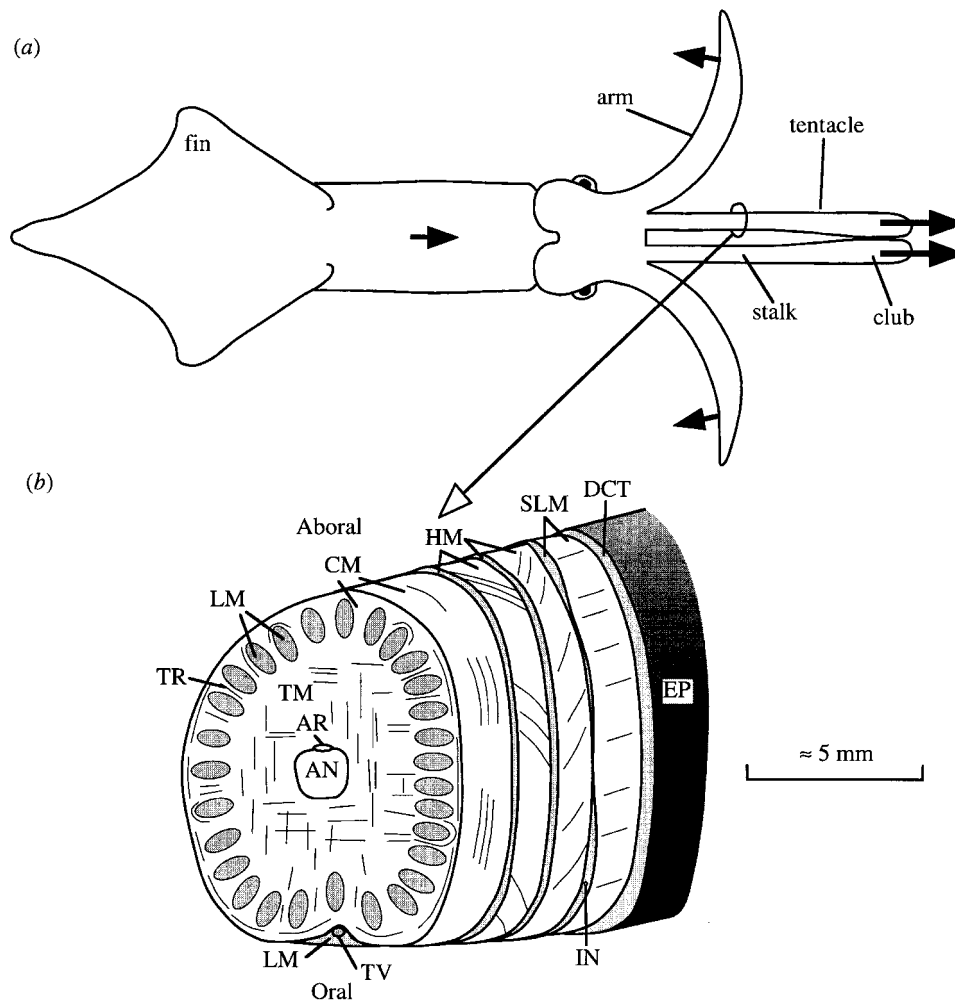
Figure 1. (*a*) Diagram of a squid. Only two of the eight arms are shown. During prey capture the squid swims forward, flares six arms outward and backward, and rapidly extends the muscular stalks of the tentacle such that the tentacular clubs are accelerated forward to attach to the prey. During much of the strike, two arms are used to stabilize the tentacles (Kier & Van Leeuwen 1997). Heavy type arrows depict directions of movement. (*b*) Diagram of the morphology of the tentacular stalk in loliginid squid (redrawn from Kier (1982)). Abbreviations: AN, axial nerve cord; AR, artery; CM, circular muscles, DCT, dermal connective tissue; EP, epithelium; HM, helical muscle; IN, intramuscular nerve cord; LM, longitudinal muscle; SLM, superficial longitudinal muscle (thickness of this layer is variable); TR, trabeculae of transverse muscle; TM, transverse muscle; TV, superficial tentacular vein.

(*a*) Model outline and geometry

We shall consider a model tentacular stalk that is divided into a longitudinal series of $n-1$ circular discs. Distally, the terminal club is represented by segment n (figure 2*a*). The terminal club is treated as a rigid element (without any muscular activity), the motion of which is determined by the activity of the muscle fibres in the stalk. The segments remain at all times connected with one another by their proximal and distal boundaries; boundary b_i is positioned between segments i and $i+1$. For reasons of simplicity, discs i and $i+1$ may have different radii at b_i. Alternatively, we could have divided the stalk into a longitudinal series of thin frustums of right circular cones (figure 2*b*). This would have led to a better connectivity between neighbouring segments, but also to much more cumbersome mathematics. Furthermore, the two approaches yield the same solution if the length of all individual stalk segments

approaches zero.

Most equations that follow will be written for one particular disc only. Parameters for one disc are given in italic symbols. When referring to all stalk segments (or segment boundaries), related bold-italic vector symbols are used, the components of which denote the parameter values for the respective segments. For instance, the acceleration vector $\boldsymbol{a} = (a_1, a_2, \ldots, a_{n-2}, a_{n-1})^{\mathrm{T}}$, where the superscript 'T' denotes the transpose.

We aim to calculate the elongation of the system of tentacular discs and the forward motion of the tentacular club as a result of the activation of the extensor muscles of the tentacular stalk. Figure 3*a* shows a highly simplified diagram of the computational scheme. Muscle stresses in the system are calculated from prescribed activation patterns and information on the instantaneous strain and strain rate using prescribed force–strain and force–strain-rate relationships as well as passive force–strain charac-

(a)

(b)

(c)

(d)
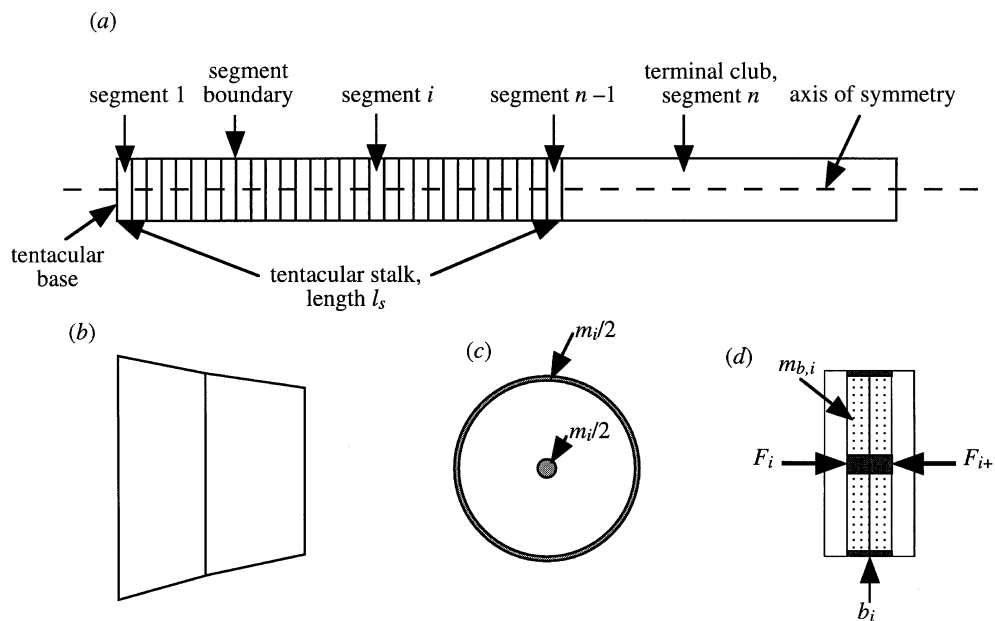
Figure 2. (a) Diagram of the model geometry, with a tentacular stalk divided in $n-1$ discs and a tentacular club of mass m_{club}. (b) Two segments with the shape of a frustum of a circular cone. Although a good connectivity between segments can be generated, this geometry was not adopted to simplify the mathematics. (c) Cross-section of segment. In the calculations, half of the segmental mass is assumed to be concentrated in the centre while the other half is assumed to be concentrated as a ring at the segmental boundary (see shaded areas). Both mass concentrations have identical longitudinal positions throughout the extension. (d) Sagittal view of two neighbouring segments. Longitudinally directed forces F_i and F_{i+1} (equation (44)) on mass $m_{\mathrm{b},i}$ (sum of darkly shaded mass concentrations) associated with boundary b_i. Mass $m_{\mathrm{b},i}$ is equal to $\frac{1}{2}(m_i + m_{i+1})$.

teristics. Viscous stresses proportional to the longitudinal strain rate are also included. The acceleration of a tentacular part is calculated by application of Newton's second law of motion. Velocities of tentacle parts are obtained from accelerations by numerical integration. From these velocities, strain rates are calculated. Positions of tentacle parts are calculated from their velocities by integration. Strains are calculated from these positions. Feedback loops in the diagram of figure 3a are included due to the strain and strain-rate dependence of the mechanical stresses in the muscle fibres. Figure 3b shows a more detailed flow diagram reflecting equations (3)–(44) described in §§ 4c, d. As will be made clear, this is an implicit scheme, which can be made explicit using the matrix equation (45), and the equations in the appendix. These last detailed considerations may be skipped by readers with a general interest only.

In the following, we first list the most important simplifying assumptions of the modelling procedure (§ 4b). Second, we define how muscle stresses are calculated (§ 4c). Third, the equations of motion of the system will be derived (§ 4d). Finally, we discuss our choice of optimization criterion for tentacle extension (§ 4e). Sections 4c and 4d are fairly mathematical. Most of what follows, however, should be comprehensible to the general biologist without a detailed understanding of §§ 4c and 4d.

(b) *Simplifying assumptions*

Any model of a biological object requires that simplifying assumptions be made. In our case, we decided on the following list of important simplifications and assumptions.

(1) Axisymmetric shape and material properties are assumed along the tentacle, although tentacles generally have (distorted) elliptical cross-sectional shapes.

(2) The actions of the thin helically arranged muscle layers are ignored.

(3) Only frictional (retarding) and passive tensile forces of the longitudinal muscle fibres are included. Thus, only the extensor muscles are assumed to be active during the strike.

(4) In each stalk segment, the circularly arranged extensor muscles are assumed to have the same activation, the same strain, and exert the same stress as the transverse muscle fibres. As in vertebrate skeletal muscles, the circularly arranged muscle fibres create a radially directed pressure gradient proportional to their curvature and tensile stress (Van Leeuwen & Spoor 1992, 1993). Nevertheless, we assume a zero pressure gradient in the radial direction because this layer of curved muscle fibres is very thin. The assumption of an equal active and mechanical state of all the extensor fibres in one segment preserves the axisymmetric condition because it avoids any buckling of the tentacle, and therefore complex considerations about the fluid and muscle dynamics. It also reduces enormously the number of possible tentacular extensions in the optimization study of myofilament lengths (see § 6). The model allows variations in the activation along the stalk. In this paper, however, the same activation pattern will be used for the

Figure 3. Flow diagrams of calculations. Algebraic steps are shown by square boxes with equation numbers where appropriate. Integration is shown by triangles, whereas boxes with rounded corners show model constants and initial conditions. Bold symbols denote vectors. (*a*) Much simplified diagram of calculations. (*b*) Diagram of calculations based on equations (3)–(44). This is an implicit scheme owing to the feedback loop from the acceleration vector $\boldsymbol{a}$. This scheme can be replaced by an explicit calculation scheme using the matrix equation (45) and the equations of the appendix.

complete tentacular stalk in all simulations.

(5) Viscous forces in the external fluid and frictional forces on the tentacle are ignored. This is reasonable due to the short duration of the extension process (about 30 ms), which is too brief for the development of a significant boundary layer. Before the tentacles elongate and the arms flare outwards, the surrounding water will be at rest relative to the tentacle. The thickness of the boundary layer around the club is likely to grow in proportion to $(\nu t)^{1/2}$ (Lighthill 1986), where ν is kinematic viscosity and t is time. A typical duration of the strike is 30 ms, while ν is about 1 mm^2 s^{-1}. This results in a boundary layer thickness of about 0.173 mm at the end of the elongation phase, which is only about 2.3% of the

tentacular diameter. This value is an estimate for the maximum thickness, which can only occur near proximal parts of the tentacle at the end of the strike. The effective added mass of a slender body like a tentacle will generally be below 10% (Lighthill 1986). For example, a Rankine ovoid of radius r and distance between source and sink of l has and added mass of water of $\rho V_{\text{body}} r / (3l - r)$, where ρ is the water density and V_{body} is the volume of considered body. Typical values for r and l are 4 mm and 45 mm, respectively. These values give an added mass of only 3.0% of the water displaced by the body. This is likely to be an underestimate because in reality the tentacle deforms. The stalk pushes the club forward together with some water. At the same time, water is sucked

towards the axis of the stalk. Numerical evaluation of the kinetic energy imparted to the water by the tentacle (space limits do not allow a detailed discussion of these calculations) resulted in an estimate of 8% for the effective added mass of water.

(6) A constant volume will be assumed for each segment of the tentacle. Muscle tissue is difficult to compress and indeed does not change volume significantly during activation (Abbott & Baskin 1962). Using the assumptions of incompressibility, a constant shape of the cross-sectional area, and homogeneous strain distributions in every cross-section along the tentacular stalk, one may derive simple relationships between the local strains in the radial and the longitudinal directions (see equation (24)).

(7) No interaction between tentacle and prey is assumed. This again avoids the calculation of complex movements.

(c) *Muscle mechanical properties*

Let us first define the nominal strain in the radial direction as

$$\varepsilon_{r,i} = (r_i - r_0)/r_0, \tag{1}$$

and for the longitudinal direction as

$$\varepsilon_{l,i} = (h_i - h_{0,i})/h_{0,i}, \tag{2}$$

where r_i is the local radius of the tentacular stalk and h_i the height of disc i. Subscripts with a 0 denote initial values. Because of assumption (4), the extensor muscle fibres of one segment may be treated as one unit. All other muscle groups are assumed to be inactive during the strike.

We will use sliding filament theory (e.g. Huxley & Niedergerke 1954) and the concept of cross-bridges as independent force generators (Gordon *et al.* 1966) to derive equations for muscle mechanical properties. Similar to the approach of Van Leeuwen (1991), we assume that the nominal tensile stress in the extensor muscles (i.e. the tensile force per cross-sectional area of the initial relaxed state) is derivable from the maximum isometric stress at optimum length σ_{max}, the normalized active state f_a, the velocity dependence function f_v, the filamentary overlap function f_l and a passive component σ_{pas}:

$$\sigma_{r,i} = f_{a,i}\sigma_{max,i}f_{v,i}f_{l,i} + \sigma_{pas,i}. \tag{3}$$

It is assumed that $f_{a,i}$ lies in the interval $[0, 1]$. A muscle fibre is fully active if $f_{a,i} = 1$, and completely inactive if $f_{a,i} = 0$. The activation is assumed to rise from zero to the maximum level, and to remain at the maximum during the remainder of the strike. A delay in the start of activation along the tentacle, which is proportional to the initial distance from the tentacular base, is also allowed. This is described by the following equations:

$$f_{a,i} = 0, \quad \text{for } t \leqslant t_{d,i}, \tag{4}$$

$$f_{a,i} = \left(\frac{1}{2}\left(1 + \sin\left(\frac{\pi(t - t_{d,i})}{t_a} - \frac{1}{2}\pi\right)\right)\right)^q,$$
$$\text{for } t_{d,i} < t < t_{d,i} + t_a, \tag{5}$$

$$f_{a,i} = 1, \quad \text{for } t \geqslant t_{d,i} + t_a, \tag{6}$$

where $t_{d,i}$ is the delay with respect to the most proximal activation, t_a is the time between the start and full activation, and q is introduced to allow a modification of a basic sinusoidal shape.

The dependence of the active force on the strain rate is described by the function f_v (figure 4a):

$$f_{v,i} = 1.8 - 0.8\frac{(1 + \dot{\varepsilon}_{r,i}^*)}{(1 - 7.56\dot{\varepsilon}_{r,i}^*/k)}, \quad \text{for } \dot{\varepsilon}_{r,i}^* < 0, \tag{7}$$

$$f_{v,i} = \frac{(1 - \dot{\varepsilon}_{r,i}^*)}{(1 + \dot{\varepsilon}_{r,i}^*/k)}, \quad \text{for } \dot{\varepsilon}_{r,i}^* \geqslant 0, \tag{8}$$

where k is a constant and $\dot{\varepsilon}_i^* = \dot{\varepsilon}_i/\dot{\varepsilon}_{min,i}$; $\dot{\varepsilon}_{min,i}$ is the minimum (unloaded) strain rate. Equation (7), as formulated by Otten (1987), is actually based on stretch experiments of vertebrate muscles (Aubert 1956). Equation (7), represents the equation of Hill (1938). Unfortunately, physiological data required for an accurate estimate of the parameter values of equations (7) and (7) are not yet available for squid muscles.

The filamentary overlap function (figure 4c) can be derived from formulae given in Van Leeuwen (1991):

$$f_{l,i} = (l_{myo,i} + l_{act,i} + l_z - l_{sarc,i})/(l_{myo,i} - l_{bz}),$$
$$\text{for } l_{act,i} + l_{bz} + l_z \leqslant l_{sarc,i} \leqslant l_{myo,i} + l_{act,i} + l_z, \tag{9}$$

$$f_{l,i} = 1, \quad \text{for } l_{act,i} + l_z \leqslant l_{sarc,i} \leqslant l_{act,i} + l_{bz} + l_z, \tag{10}$$

$$f_{l,i} = (l_{myo,i} - l_{bz} - D_{act}(l_{act,i} + l_z - l_{sarc,i}))$$
$$\times (l_{myo,i} - l_{bz})^{-1},$$
$$\text{for } l_{myo,i} + l_z \leqslant l_{sarc} \leqslant l_{act,i} + l_z, \tag{11}$$

$$f_{l,i} = (l_{myo,i} - l_{bz} - D_{act}(l_{act,i} + l_z - l_{sarc,i})$$
$$- D_{myo}(l_{myo,i} + l_z - l_{sarc,i}))/(l_{myo,i} - l_{bz})$$
$$- C_{myo}(l_{myo,i} + l_z - l_{sarc,i})/(l_{myo,i} - l_{bz}),$$
$$\text{for } l_{min,i} \leqslant l_{sarc,i} \leqslant l_{myo,i} + l_z. \tag{12}$$

In these equations, $l_{act,i}$ is the summed length of two opposing actin filaments in one sarcomere, $l_{myo,i}$ is the myosin filament length, l_{bz} is the length of the bare zone on the myosin filament, l_z is the width of the Z-disc, and $l_{sarc,i}$ is the sarcomere length (figure 4e). Furthermore, D_{act} and D_{myo} are parameters to account for cross-bridge losses owing to actin overlap and interaction between myosin filament and Z-disc. Finally, C_{myo} is introduced to account for resistive forces as a result of the collision of the myosin filaments with the Z-disc of the sarcomere. These parameters were discussed in detail by Van Leeuwen (1991). Along the stalk, l_{act}, l_{myo} and l_{sarc} can vary, whereas l_{bz} and l_z are kept constant. The optimum sarcomere length for active force production is defined as

$$l_{0sarc,i} = l_{act,i} + l_z + \tfrac{1}{2}l_{bz}. \tag{13}$$

We assume that all sarcomeres have length l_{0sarc} in the initial relaxed state of the tentacle and also that in one segment all sarcomeres have the same length, so that $l_{sarc,i}$ can be calculated from

$$l_{sarc,i} = l_{0sarc,i} + \varepsilon_{r,i}l_{0sarc,i}. \tag{14}$$
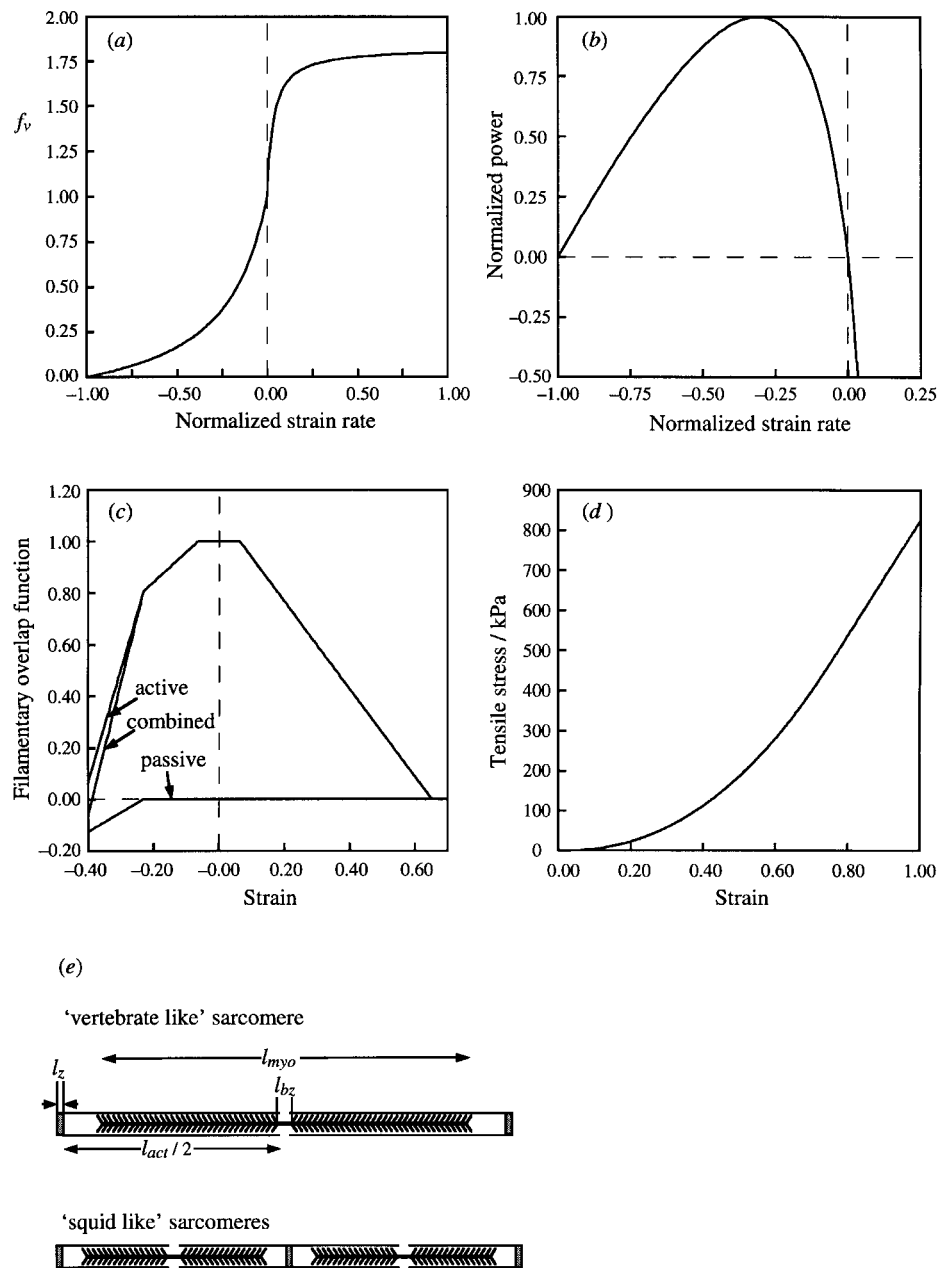
Figure 4. (*a*) Velocity dependence function f_v against normalized strain rate $(-\dot{\varepsilon}/\dot{\varepsilon}_{\min})$ (equations (7) and (7)). A value of 0.25 is chosen for k. (*b*) Normalized power (with respect to peak power) as a function of normalized strain rate. (*c*) Filamentary overlap function according to equations (9)–(9). (*d*) Passive stress-strain relationship as defined by equations (17)–(17), with the parameter values of table 1. (*e*) Illustration of sarcomere geometry with a length comparison between a typical vertebrate sarcomere and a typical tentacle sarcomere. The squid sarcomere produces the smaller force (tensile stress) due to the smaller number of available myosin heads, but it can generate the stronger negative unloaded strain rate due to the short sarcomere length. In a gross-morphological design which results in a very low (local) tissue load, the squid sarcomere is the better design because relatively high strain rates can be generated with interfilamentary sliding speeds that are (close to) optimal for power output.

In our optimization study of myofilament lengths, we assume that

$$\sigma_{\max,i} \propto l_{\mathrm{myo},i} - l_{\mathrm{bz}}, \qquad (15)$$

and that

$$\dot{\varepsilon}_{\min,i} \propto l_{\mathrm{0sarc},i}^{-1}. \qquad (16)$$

Equation (15) follows from the fact that the number of cross-bridges is proportional to $l_{\mathrm{myo},i} - l_{\mathrm{bz}}$. Equation (16) follows from the fact that the maximum

shortening speed of a muscle fibre is proportional to the number of sarcomeres in series.

Finally, the passive component in equation (3) was formulated as

$$\sigma_{\mathrm{pas},i} = 0, \quad \text{for } \varepsilon_i \leqslant 0, \qquad (17)$$

$$\sigma_{\mathrm{pas},i} = c_{1\mathrm{pas}}\varepsilon_i^{c_{2\mathrm{pas}}}, \quad \text{for } 0 < \varepsilon_i < \varepsilon_{\mathrm{c}}, \qquad (18)$$

$$\sigma_{\mathrm{pas},i} = c_{3\mathrm{pas}}\varepsilon_i + c_{4\mathrm{pas}}, \quad \text{for } \varepsilon_i \geqslant \varepsilon_{\mathrm{c}}, \qquad (19)$$

where ε_{c} is the critical strain above which the relationship is linear, and $c_{1\mathrm{pas}}, \ldots, c_{4\mathrm{pas}}$ are constants.

Furthermore, ε_i stands either for $\varepsilon_{l,i}$ or for $\varepsilon_{r,i}$. To ensure a connection with a continuous first derivative at ε_c, we defined c_{1pas} and c_{2pas} as

$$c_{1pas} = \frac{c_{3pas}}{c_{2pas}\varepsilon_c^{c_{2pas}-1}}, \tag{20}$$

$$c_{2pas} = \frac{c_{3pas}\varepsilon_c}{c_{3pas}\varepsilon_c + c_{4pas}}. \tag{21}$$

Viscous effects in the extensor muscles are only taken account of by the velocity dependence function. In the longitudinal muscles, we introduce a viscous counter force which is thought to be caused primarily by sliding of myofilaments (see next subsection).

(d) Modelling the tentacular dynamics

Let the total length of the tentacular stalk be l_s. Naturally, the local radius r_i can vary with the segmental position along the stalk and with time. Let r_0 and l_{s0} be the values of r_i and l_s in the relaxed zero-strain condition. No tapering is assumed in the initial state of the stalk. Therefore, r_0 is the same along the stalk. Tapering can, however, occur during the extension phase. We begin by calculating the volume of a tentacular disc because from the constancy of local volume important relationships can be derived between the tentacular motions in the longitudinal and in the radial direction. The volume of disc i is

$$V_i = \pi h_i r_i^2, \tag{22}$$

where h_i is the height of the disc. From the constancy of volume, it follows that $\pi h_i r_i^2 = \pi h_{0,i} r_0^2$; hence,

$$r_i = r_0(h_{0,i}/h_i)^{1/2}. \tag{23}$$

We can express (using (23)) the radial strain as a function of the longitudinal strain:

$$\varepsilon_{r,i} = (1 + \varepsilon_{l,i})^{-1/2} - 1. \tag{24}$$

Differentiation of (24) gives the relation between the radial and longitudinal strain rates:

$$\dot{\varepsilon}_{r,i} = -\tfrac{1}{2}(1 + \varepsilon_{l,i})^{-3/2}\dot{\varepsilon}_{l,i}. \tag{25}$$

As is apparent from (24) and (25), the radial strain and strain rate do not depend on the initial ratio of radius and length of the stalk. This result contradicts the suggestion by Kier & Smith (1985) that tentacles with relatively small *initial* radii would require relatively small (absolute) radial strain rates for the production of a particular longitudinal strain rate. The above formula, however, does suggest that, for a given longitudinal strain rate, the required radial strain rate becomes less negative during tentacle lengthening (figure 5b). Nevertheless, slender tentacles have some distinct advantages that will be addressed later.

Each disc keeps constant volume (assumption (6)); thus,

$$\dot{V}_i = \frac{\mathrm{d}\pi r_i^2 h_i}{\mathrm{d}t} = \pi(2r_i h_i \dot{r}_i + r_i^2 \dot{h}_i) = 0. \tag{26}$$

Hence,

$$\dot{r}_i = -\frac{\dot{h}_i r_i}{2h_i}. \tag{27}$$

Now let l_i be the position of boundary b_i, u_i its velocity, and a_i its acceleration, so that

$$h_i = l_i - l_{i-1}, \tag{28}$$

$$\dot{h}_i = u_i - u_{i-1}, \tag{29}$$

$$\ddot{h}_i = a_i - a_{i-1}. \tag{30}$$

Equation (27) can now be rewritten as

$$\frac{u_i - u_{i-1}}{l_i - l_{i-1}} = \frac{-2\dot{r}_i}{r_i}. \tag{31}$$

If $h \to 0$ mm, we obtain from (31):

$$\frac{\mathrm{d}u}{\mathrm{d}l} = \frac{-2\dot{r}}{r}, \tag{32}$$

where u is the velocity in the longitudinal direction. By application of the chain rule for differentiation to (27), the radial acceleration of the circumferential disc boundary is calculated as

$$\ddot{r}_i = -\frac{1}{2}\left(\frac{\dot{h}_i \dot{r}_i}{h_i} - \frac{r_i \dot{h}_i^2}{h_i^2} + \frac{r_i \ddot{h}_i}{h_i}\right). \tag{33}$$

Together, equations (27) and (33) define the relationships between the longitudinal and the radial segmental motions. Below, we will show how the forward acceleration of the system can be calculated using Newton's second law of motion. To do so, we first need to know the effective mass for the acceleration of the lateral surface boundary of segment i. This is required for two reasons. First, we have avoided any subdivision of the stalk in the radial direction. Second, some surrounding water will be accelerated with the tentacle surface. For the first aspect, it is useful to calculate the kinetic energy of the disc associated with the radial contraction only, which can be derived by integration over the tissue mass (and by noting from equation (27) that $\dot{r} = \dot{r}_i r/r_i$):

$$E_{kr,i} = \int_0^{r_i} \frac{2\pi r h_i \rho}{2}\dot{r}^2\,\mathrm{d}r = \frac{\pi h_i \rho \dot{r}_i^2}{r_i^2}$$
$$\times \int_0^{r_i} r^3\,\mathrm{d}r = \tfrac{1}{4}\pi r_i^2 h_i \rho \dot{r}_i^2 = \tfrac{1}{4}m_i \dot{r}_i^2, \tag{34}$$

where ρ is the density of the tissue, and m_i is the mass of disc i:

$$m_i = \pi r_0^2 h_{0,i}\rho = \pi r_i^2 h_i \rho. \tag{35}$$

Equation (34) shows that half the disc mass can be assumed to lie at the circumferential boundary in a calculation of the radial acceleration of this boundary. The other half should then be assumed to be concentrated at the axis of symmetry of the tentacle (figure 2c). Now, we need also to add a particular mass of water. For reasons of simplicity, we prefer to take a fixed fraction α of the disc mass. The force on both masses equals the outer surface area $A_{s,i}$ of the disc multiplied by the difference between the intramuscular pressure and a fraction η of the muscle fibre stress $\sigma_{r,i}$, where we have ignored the external fluid pressure and any pressure gradient in the radial direction in the tentacle. We take only a fraction of the fibre stress because the volume is only partially filled with fibres. Hence, for the radial direction,

$$A_{s,i}p_i - \eta A_{s0,i}\sigma_{r,i} = m_i(\tfrac{1}{2} + \alpha)\ddot{r}_i, \tag{36}$$
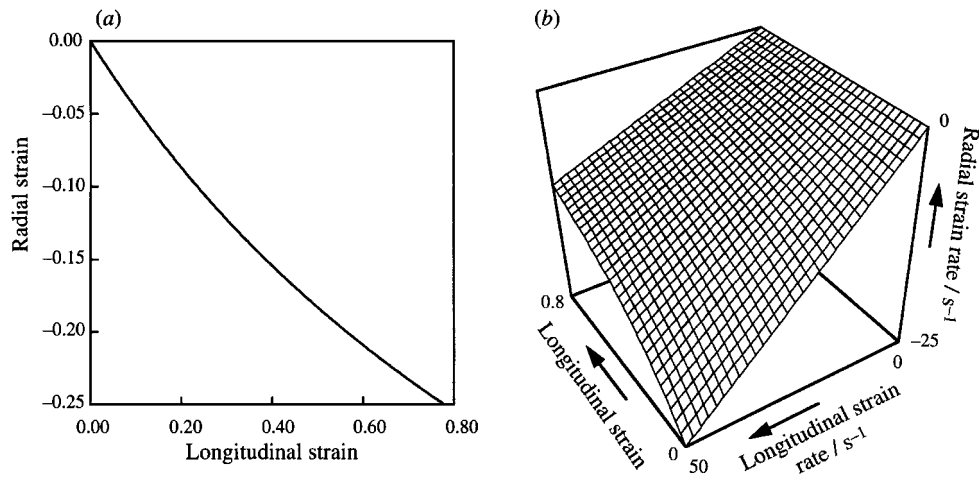
Figure 5. (*a*) Relationship between longitudinal and radial strain in a tentacular segment according to equation (24). (*b*) Relationship between longitudinal and radial strain rates in a tentacular segment according to equation (25).

where

$$A_{s,i} = 2\pi r_i h_i. \tag{37}$$

The initial surface $A_{s0,i}$ is used in conjuction with the muscle stress because we work with nominal stresses. By rewriting (36), an equation is derived for the intramuscular pressure:

$$p_i = \frac{\eta A_{s0,i}\sigma_{r,i} + m_i(\frac{1}{2} + \alpha)\ddot{r}_i}{A_{s,i}}. \tag{38}$$

We now need to derive expressions for the elongation of the segments by calculating the accelerations of the (cross-sectional) boundaries between adjacent discs. The mass associated with boundary b_i (figure 2*c*) is calculated as

$$m_{b,i} = \tfrac{1}{2}(m_i + m_{i+1}), \qquad 1 \leqslant i \leqslant n - 2. \tag{39}$$

We assume that the longitudinal forces will be equally distributed over the central and the peripheral mass concentrations (figure 2*c,d*). The mass at boundary b_{n-1} between the terminal stalk segment and the terminal club (with mass $m_n = m_{club}$), is prescribed by

$$m_{b,n-1} = \tfrac{1}{2}m_{n-1} + m_{club} + \alpha m_{club}, \tag{40}$$

where we have again introduced an added mass term. The cross-sectional area of disc i is

$$A_{c,i} = \pi r_i^2. \tag{41}$$

A pressure force of magnitude $p_i A_{c,i}$ acts on the proximal side of $m_{b,i}$, whereas a force $-p_{i+1}A_{c,i+1}$ pushes against the distal side of $m_{b,i}$. Likewise, tensile forces $-\sigma_{l,i}A_{cl0}$ and $\sigma_{l,i+1}A_{cl0}$ operate on the lower and upper sides owing to tensile stresses originating from stretched muscle and connective tissue fibres (A_{cl0} is reference cross-section of longitudinal muscle group). Finally, force components $-\dot{\varepsilon}_{l,i}\mu A_{cl0}$ and $\dot{\varepsilon}_{l,i+1}\mu A_{cl0}$ act on the proximal and distal sides. These forces originate mainly from friction between sliding long myofilaments of the obliquely striated longitudinal muscle fibres. If F_i is defined as

$$F_i = A_{c,i}p_i - A_{cl0}(\sigma_{l,i} + \dot{\varepsilon}_{l,i}\mu), \quad \text{for } 1 \leqslant i \leqslant n - 2, \tag{42}$$

$$F_i = 0, \quad \text{for } i = n - 1, \tag{43}$$

we can write the acceleration a_i of boundary b_i as

$$a_i = (F_i - F_{i+1})/m_{b,i}. \tag{44}$$

Expression (44) is in fact an implicit equation for a_i, because F_i and F_{i+1} depend on $\ddot{r}_i$ and $\ddot{r}_{i+1}$, whereas, in equation (33), $\ddot{h}_i = a_i - a_{i-1}$. After some algebra, it follows that the acceleration vector $\boldsymbol{a}$ can now be obtained by solving the matrix equation

$$
\begin{bmatrix}
c_{2,1} & c_{3,1} & 0 & \cdots & & & \\
c_{1,2} & c_{2,2} & c_{3,2} & \cdots & & & \\
 & & \cdots & & & & \\
 & & \cdots & c_{1,n-2} & c_{2,n-2} & c_{3,n-2} & \\
 & & \cdots & 0 & c_{1,n-1} & c_{2,n-1} &
\end{bmatrix}
\begin{bmatrix}
a_1 \\ a_2 \\ \cdots \\ a_{n-2} \\ a_{n-1}
\end{bmatrix}
$$

$$
=
\begin{bmatrix}
c_{4,1} \\ c_{4,2} \\ \cdots \\ c_{4,n-2} \\ c_{4,n-1}
\end{bmatrix}. \tag{45}
$$

Expression (45) is a tridiagonal system of linear equations, i.e. the matrix in (45) has non-zero elements only in the diagonal-plus or minus-one column. The system is tridiagonal because each boundary mass has direct mechanical interactions only with its two (proximal and distal) direct neighbours (see force diagram of figure 2*d*). The components c are fairly lengthy algebraic expressions which can be calculated by respective substitution of (33) in (38), (38) in (42), and finally (42) in (44). These expressions, the values of which change with time, are derived in the appendix.

From (42), it is clear that $F_i \propto A_{c,i}$, but also $m_{b,i} \propto A_{c,i}$. These proportionalities suggest that an enlargement of the radius would have no effect on the acceleration capabilities of the tentacle (equation (44)). With an increasing radius, we expect, however, a slight decrease in the accelerations owing to a relatively larger added mass of water (which can be adjusted by choosing a larger value for α).

(e) Defining object functions for optimization

Natural selection probably favours tentacular designs that provide a relatively high probability of prey capture. Extensions with a high average velocity before prey contact (and thus a fairly high initial acceleration) are probably very effective because they minimize the available response (escape) time of the prey. The optimum moment of contact between tentacle and prey, however, is difficult to determine. It may not be optimal if the prey is hit at the instant of maximum club velocity because the considerable impact may hinder attachment of the suckers to the prey. On the other hand, prey attachment at full extension may be even more unfavourable, because of the zero velocity of extension (the clubs would still have some speed due to forward swimming). The optimal moment of prey attachment is probably between these two extremes, and is likely to depend also on the nature (e.g. mass and shape) of the prey. The requirement of a maximization of the mean extension velocity is expected to yield design predictions very close to a maximization of the peak velocity (and thus the peak kinetic energy) of the tentacular club because the peak extension is only slightly variable owing to the (fixed) visco-elastic properties of the tentacle. Maximization of the peak velocity was chosen for our optimization study, because it is relatively easy to implement while it avoids in this initial study the introduction of prey characteristics. We have not chosen peak acceleration as our optimization criterion because this would predict sarcomere designs with very long myofilaments that can produce a very high tensile stress, at the expense of a very low maximum contraction velocity.

In summary, myofilament lengths along the tentacular stalk will be adjusted so as to maximize the peak velocity of the terminal club. In this procedure, we will assume that we can derive $\sigma_{\max}$ (using equation (15)) from

$$\sigma_{\max,i} = \sigma_{\max,\mathrm{ref}}(l_{\mathrm{myo},i} - l_{\mathrm{bz}})/(l_{\mathrm{myo,ref}} - l_{\mathrm{bz}}), \quad (46)$$

where $\sigma_{\max,\mathrm{ref}}$ is the maximum isometric tension of a reference sarcomere with a thick filament length of $l_{\mathrm{myo,ref}}$. Similarly, $\dot{\varepsilon}_{\min,i}$ is calculated from

$$\dot{\varepsilon}_{\min,i} = \dot{\varepsilon}_{\min,\mathrm{ref}} l_{0\mathrm{sarc,ref}}/l_{0\mathrm{sarc},i}, \quad (47)$$

where $\dot{\varepsilon}_{\min,\mathrm{ref}}$ is the minimum unloaded shortening velocity of the same reference sarcomere with an optimum sarcomere length of $l_{0\mathrm{sarc,ref}}$. In the optimization study, the most proximal and the most distal filaments were varied, while the lengths for intermediate positions were derived by linear interpolation. This choice is suggested by the linear decrease of the distal tentacular mass with distance from the tentacular base and the enormous reduction in the number of possible variations in filament lengths.

5. NUMERICAL PROCEDURES

The second-order differential equation (44) can be written as two first-order differential equations by realizing that $\dot{u}_i = a_i$ and $\dot{l}_i = u_i$. Thus, for each seg-

mental boundary we have two state variables u_i and l_i. Consequently, for a system of n segments (with $n-1$ discs and $n-1$ intersegmental boundaries), we need to solve $2(n-1)$ coupled first-order differential equations. A solution of this system requires the prescription of two boundary conditions, e.g. one at the base of the tentacle and one at the tip. For the base, we have chosen to prescribe the forward velocity of the squid. In practice, we took a constant value. For the tip, we took the pressure to be zero. It should be realized that a hydrodynamic pressure acts at the tentacular club. We have simulated this with the added mass term in (40). The $2(n-1)$ differential equations were solved using an (iterative) Crank–Nicolson integration procedure. This implicit approach is second-order accurate in time and provides good stability (Press *et al.* 1989). At each considered time instant, the tridiagonal system (45) was solved using the Pascal procedure Tridag (Press *et al.* 1989).

Program development was done in Pascal on a MacIntosh Quadra 800 system (Apple). Final runs were made on an AXP 3000s M600 system (Digital), using IEEE double-precision accuracy. Test runs were made on both platforms, yielding only non-significant differences in the solutions. Test runs were also made with different values of the time step. Final runs were made with a time step that resulted in a deviation of less than 0.1%. In the test runs, the number of segments n was also varied. It was found that about 50 segments were required for an accuracy of 0.1% in prediction of optimum filament lengths (the higher the number of segments, the greater the predicted difference in filament length between base and tip of the tentacular stalk). Optimum filament lengths were searched using the downhill simplex method of Nelder & Mead (1965), as implemented in the Pascal procedure Amoeba (Press *et al.* 1989). Taking relatively long or relatively short myofilaments at the tip or base (as compared to the optimal design) leads to an unstable tentacular stalk, i.e. particular segments are compressed by the activity of other relatively stronger segments along the stalk. Interestingly, relatively short time steps in the integration procedure are required for an accurate calculation of this mechanical instability phenomenon.

6. RESULTS AND DISCUSSION

In this section, we shall first discuss briefly the kinematics of a high-speed filmed tentacle strike. Second, we shall show the results of a simulated tentacle strike that approximates the fastest event. Finally, the results of an optimization study of the myofilament lengths will be described. The values that were assigned to the various parameters in the simulations are given in table 1.

(a) Kinematics of tentacle extension

The results of a kinematic analysis of the fastest strike recorded (Kier & Van Leeuwen 1997) are shown graphically in figure 6. We have chosen the
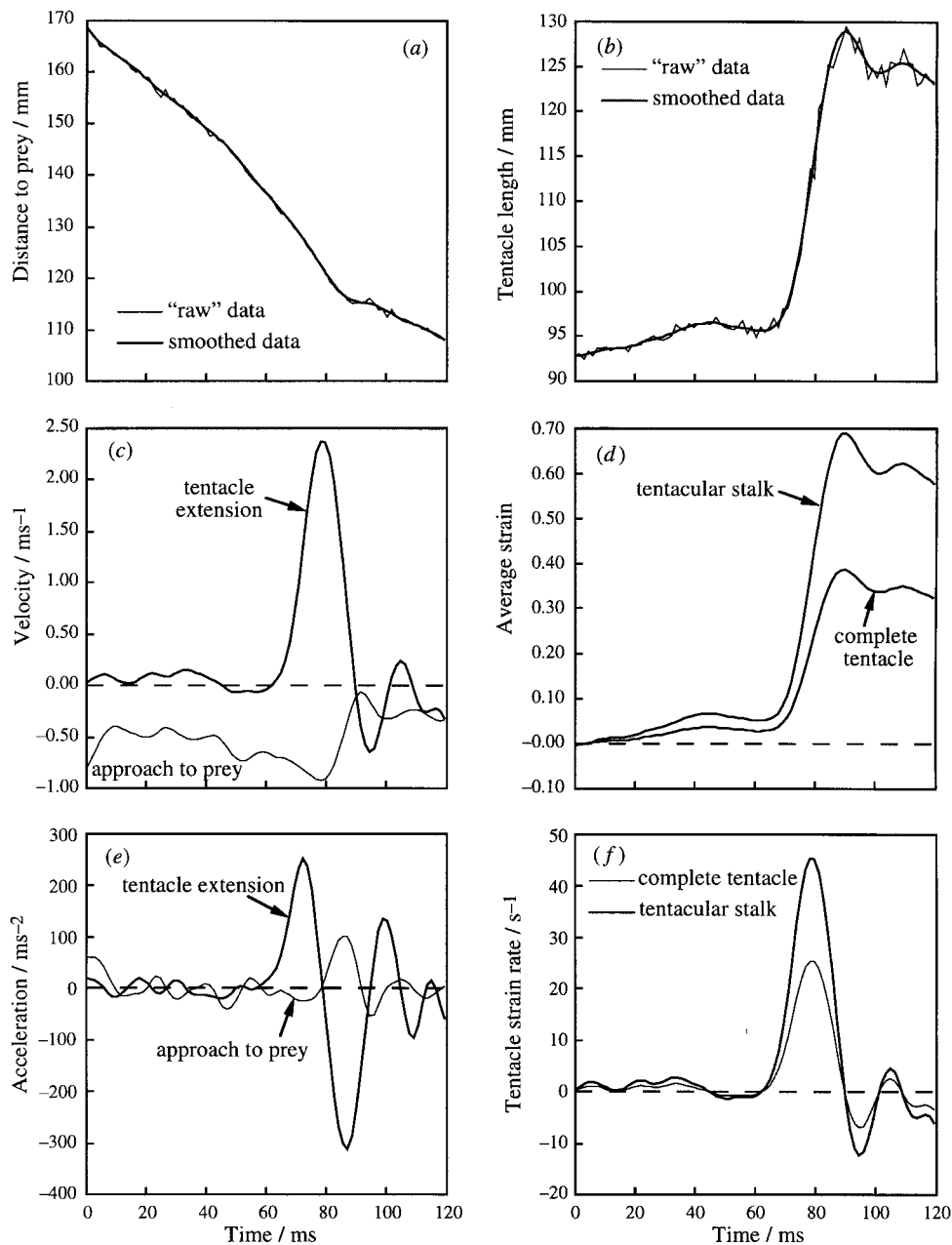
Figure 6. Results of a kinematic analysis of prey capture in a specimen of *Loligo pealei*. Thin curves in (*a*) and (*b*) show measurements from a high-speed movie, whereas the other curves in these panels were derived by quintic spline smoothing. The curves in the other panels were calculated from these smoothed curves. Due to buckling of the tentacular stalk and contact with the prey, data are inaccurate for the last 25 ms. (*a*) Body displacement. (*b*) Tentacle length. (*c*) Velocity of the tentacular tip with respect to the base of the tentacle. Velocity of body approach to prey. (*d*) Average longitudinal strain of the complete tentacle and the tentacular stalk. Strain of stalk was obtained by assuming zero strain in club. (*e*) Acceleration of the tentacular tip with respect to the base of the tentacle. Acceleration of body approach to prey. (*f*) Average longitudinal strain rate of the complete tentacle and the tentacular stalk.

fastest event because such a strike imposes the highest dynamic loads on the system. We expect the tentacular design to be most critically influenced by the maximum performance. For a more detailed discussion of tentacle kinematics, we refer to Kier & Van Leeuwen (1997). The maximum measurement error in the positional data is about 1 mm, resulting in possible errors of about 2 mm for length measurements. Therefore, quintic spline smoothing was applied before velocities and accelerations were calculated (see § 3). The accelerations have the lowest accuracy owing to the required double differentiation which tends to magnify errors.

Figure 6*a* shows the distance between a point halfway between the eyes of the squid and the prey. For much of the strike, the graph gives a reasonable representation of the body displacement because the prey had almost zero velocity up to the moment it was hit by the clubs. The slope of the curve becomes steeper until about 78 ms, then the slope decreases rapidly. The slope is a measure of the velocity which is shown by the thin curve in figure 6*c* (a negative

Table 1. *Values of constants and variables of tentacle model as used and produced in the simulations*

(The mass of the club was 0.75 of the total mass of the stalk. 15% of the cross-section was assumed to be filled with longitudinal muscles.)

symbol	value	unit
	input	
c_{1pas}	887.4	kPa
c_{2pas}	2.260	
c_{3pas}	1450	kPa
c_{4pas}	-625.0	kPa
C_{myo}	0.44	
D_{act}	0.68	
D_{myo}	1.90	
$h_{0,i}$ (in stalk)	1.063	mm
$h_{0,n}$	39.857	mm
k_{mus}	0.25	
$l_{0sarc,1}$	1.3399	μm
$l_{0sarc,n-1}$	0.7276	μm
$l_{0sarc,ref}$	2.37	μm
$l_{act,1}$	0.5976	μm
$l_{act,n-1}$	1.2099	μm
l_{bz}	0.14	μm
$l_{myo,1}$	0.9707	μm
$l_{myo,n-1}$	0.4997	μm
$l_{myo,ref}$	1.58	μm
l_{s0}	53.143	mm
l_z	0.06	μm
m_{club}	1.80	g
m_l	45.15	mg mm^{-1}
n	51	
q	15	
r_0	3.7	mm
t_a	40	ms
$t_{d,n-1}$	0	ms
α	0.08	
ε_c	0.773	
$\dot{\varepsilon}_{min,1}$	-30.07	s^{-1}
$\dot{\varepsilon}_{min,n-1}$	-55.37	s^{-1}
$\dot{\varepsilon}_{min,ref}$	-17	s^{-1}
η	0.7	
μ	38 000	g mm^{-1} s^{-1}
ρ	1050	kg m^{-3}
$\sigma_{max,1}$	161.53	kPa
$\sigma_{max,n-1}$	69.94	kPa
$\sigma_{max,ref}$	280	kPa
	output	
a_{max}	248	m s^{-2}
E_{kmax}	5.08	mJ
u_{max}	2.377	m s^{-1}
ε_{lmax}	0.641	
ε_{rmin}	0.219	

value indicates a decreasing distance between predator and prey). A peak negative velocity of about -0.9 m s^{-1} is observed. Likewise, figure 6e shows the acceleration of the body to the prey. A fairly strong negative acceleration peak (about -30 m s^{-2}) occurs just before the initiation of rapid tentacular extension.

Figure 6b shows the tentacular length through time. First, a slow and moderate extension is generated, followed by a very slight shortening. Then a very rapid lengthening follows which is completed within about 30 ms. The longitudinal strain, averaged over the complete tentacle is shown in figure 6d. On the same plot, the average strain over the tentacular stalk is shown, which was obtained by subtracting the club length from the total tentacle length. The peak average strain in the stalk is about 0.69. Even this high value is probably an underestimate because we did not correct for a slight buckling of the stalk which occurred in the final phase of the extension as the tentacles contacted the prey.

The corresponding average longitudinal strain rates are shown in figure 6f. The highest longitudinal strain rate in the stalk is about 45 s^{-1}, which corresponds to a peak strain rate for the extensor muscles of about -14 s^{-1} (calculated from equation (25)). Taking a typical half sarcomere length for the extensor muscle as 0.66 μm, a peak interfilamentary velocity of -9.24 μm s^{-1} is calculated. This value is high, but not unprecedented. If, however, the squid had a half sarcomere length of 1.10 μm, which is typical for vertebrates, a value of -15.4 μm s^{-1} would result. Thus, the short squid sarcomeres reduce considerably the required interfilamentary velocity, and the very high longitudinal strain rate can be generated with realistic sliding velocities between the actin and myosin filaments of the extensor muscles.

Considerable sliding velocities occur, however, in the obliquely striated longitudinal muscle fibres which are elongated during the strike. A typical half sarcomere length for these fibres is 2 μm, which in combination with the peak strain rate of 45 s^{-1}, results in a peak interfilamentary velocity of 90 μm s^{-1}, roughly 10 times the absolute value of the extensor muscles! These rough calculations emphasize that viscous energy losses are expected to occur mainly in the longitudinal muscles, in spite of their fairly small volume. Recall, that we were able to calculate average values only for the filmed event. In reality, peak strain rates will occur at different instances along the stalk. Therefore, peak local strain rates may be somewhat higher than the values above.

(b) Simulation of tentacle extension

Now, we shall discuss a simulated tentacle strike which roughly corresponds to the kinematic events shown above. For the simulation, myosin filament lengths were chosen that were found to be optimal for the peak velocity of the tentacular club (§ 6c). In this simulation, and in all other simulations that will follow, the sarcomere length $l_{0sarc,i}$ in each segment was taken to be $1.3(l_{myo,i} + l_z)$, and, from equation (13),
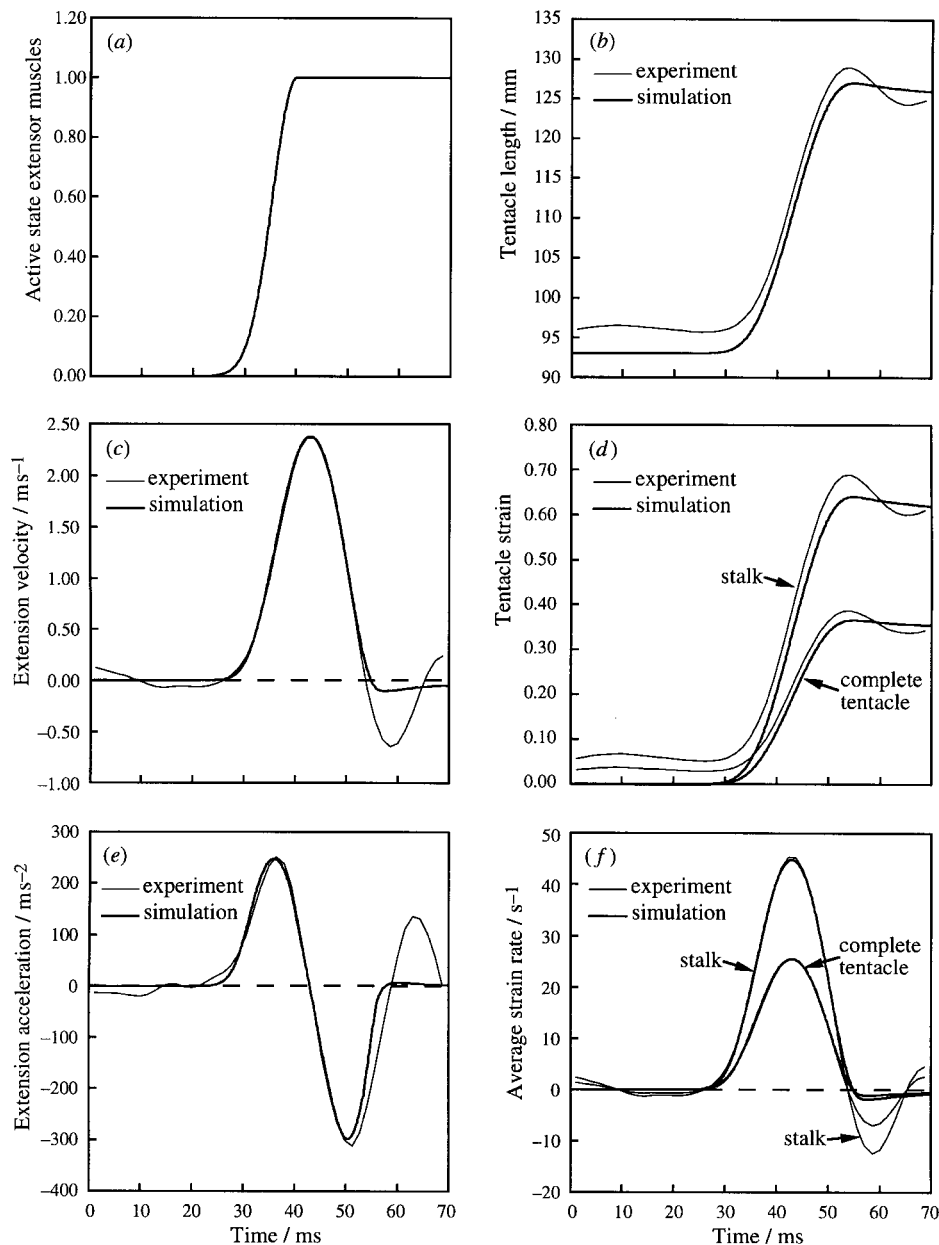
Figure 7. Comparison between the kinematic analysis of prey capture of figure 6 (*Loligo pealei*) with a model simulation. Number of model segments is 51. Curves with the standard thickness show results obtained by the present forward dynamics simulation. Thin curves represent smoothed results from a high-speed movie. (*a*) Normalized active state of the extensor muscles. All extensor fibres are given the same activation throughout the strike, all other muscle fibres are assumed to be inactive. (*b*) Tentacle length. (*c*) Velocity of the tentacular tip with respect to the base of the tentacle. (*d*) Average longitudinal strain of the complete tentacle and the tentacular stalk, respectively. (*e*) Acceleration of the tentacular tip with respect to the base of the tentacle. (*f*) Average longitudinal strain rate of the complete tentacle and the tentacular stalk, respectively. Significant differences are found between experiment and simulation after about 55 ms because of inaccuracies in the film analysis and uncertainties about muscle activation characteristics.

$l_{\text{act},i} = l_{0\text{sarc},i} - l_{\text{z}} - \frac{1}{2}l_{\text{bz}}$. The position of the base of the tentacle was kept constant in the simulation.

Figure 7 shows a comparison of the observed kinematic features in the squid *Loligo pealei* and the simulations. The events are fairly similar, both in peak values of the curves and the shapes of the curves. This should not be very surprising since we have adjusted (by hand, a formal optimization of all unknown parameters was judged to be not very useful) several physiological parameters for which no data were available so as to obtain similar extension veloc-

ities of the tentacle in simulation and experiment. Effectively, we had, given the scanty physiological data, no other choice than parameter adjustment. On the other hand, the adjusted parameters are presently the best available estimates for the muscle properties.

In the simulation, all parameter values lie within widely accepted physiological limits. For instance, the maximum interfilamentary velocity is comparable to a vertebrate muscle fibre with a minimum unloaded strain rate of $-17\ \text{s}^{-1}$, which is fairly fast,

but still below some of the most extreme values for vertebrates (Woledge *et al.* 1985). The most characteristic parameter values are the remarkably short myofilament lengths. At the tip of the stalk, l_{myo} is $0.500\,\mu m$, and at the base $0.971\,\mu m$. This length range corresponds remarkably well to the range of values $(0.5-0.9\,\mu m)$ reported in the literature (Kier 1991).

Figure 7*a* shows that the prescribed active state of the extensor muscles rises from zero to the maximum value of 1. Thus, all of the extensor muscles are assumed to have the same active state. The rise time of the activation (i.e. the time between 0.1 and 0.9 of the maximum value) is 7.72 ms. We did not attempt to simulate the slow initial rise in tentacle length seen in the experiment (figure 6*b*); the simulated rapid extension starts only very slightly above the starting length (figure 7*b*) and very slightly above the zero longitudinal average strain of both the complete tentacle and the stalk (figure 7*d*). The peak longitudinal strains in the stalk and the complete tentacle (averaged over the complete length of the structures) were therefore slightly below the corresponding peak values of the experiment.

Figure 7*c* shows the expected similarity between experiment and simulation in the extension velocities during the most rapid part of the strike. As expected from figure 7*c*, the longitudinal strain rates of the complete tentacle and of the stalk (again averaged over the complete length of the structures) are similar to the experimental values during the rapid extension phase (figure 7*f*). A similar statement can be made for the acceleration of tentacle extension (figure 7*e*). The peak negative acceleration is, in absolute terms, greater than the peak positive acceleration. This can be explained as follows. Initially, the kinetic energy in the tentacle rises until the peak extension velocity is reached. This rise in kinetic energy originates from the work done by the extensor muscles. Fairly small amounts of energy are respectively degraded to heat (see the friction term of equation (42)) and stored as elastic energy. The (retarding) elastic term in equation (42) increases in a nonlinear way (figure 4*d*). Therefore, this energy absorbing influence rises more and more rapidly during the extension phase. Finally, the elastic tissue absorbs the kinetic energy more rapidly than it was liberated by the extensor muscles. Compared to the experiment, we have exaggerated slightly the elastic effect because we simulated a similar extension to that of the experiment, but we have not compensated in the experimental calculations for the observed buckling effects or prey contact. The deviations between experiment and simulation are largest at the end of the strike (figure 7, $t > 53$ ms). This is not surprising owing to the complex final buckling in the experiment and the great uncertainties in the final muscle activities. In reality, the extensor muscles may reduce their active state once full extension is reached (in contrast to the simulation as seen in the curve of figure 7*a*). In the simulation, the final solution approaches a perfect balance between tensile forces in the extensor muscles and tensile forces in the longitudinal elastic
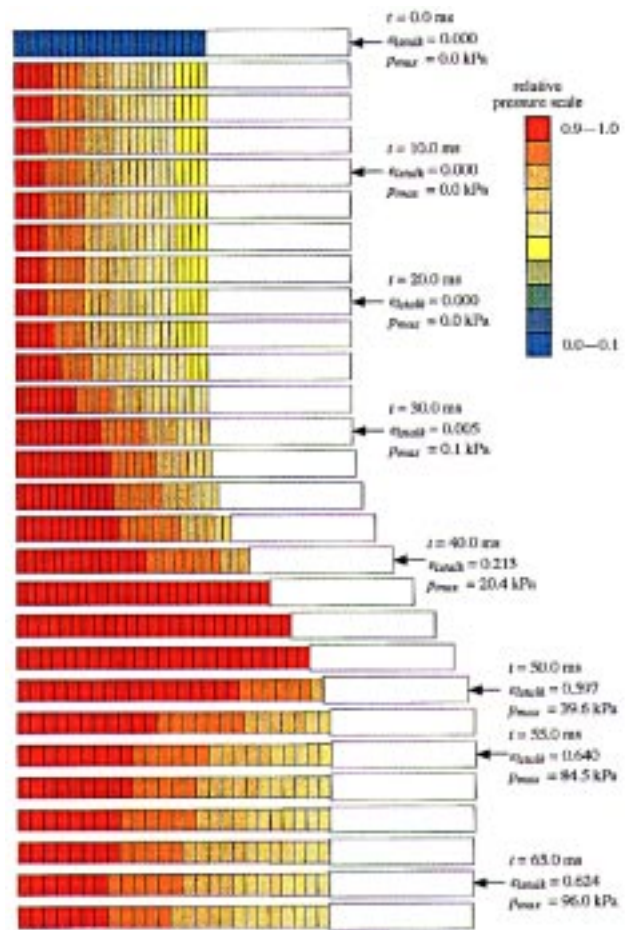
Figure 8. Simulation of tentacle deformation and internal pressure distribution in the tentacular stalk. Number of tentacular segments is 26. The pressure is scaled relative to the instantaneous maximum value in the stalk. This maximum is given together with the time of the selected instances. The same activation was prescribed along the whole tentacular stalk. The pressure gradient is negative over much of the strike, which causes a forward acceleration of the tentacular segments. However, just before full extension (43.3–47.4 ms) it is slightly positive (not resolved by the colour gradient). This decelerates tentacular extension together with elastic and viscous counter forces.

elements. This is caused by the continuing activation of the extensors and the inactivity of the rest of the muscles.

Figure 8 shows the shape and the internal pressure distribution of the tentacle for the same simulation as in figure 7 for a series of time steps (2.5 ms interval). Pressure values are given relative to the ambient pressure. At the start ($t = 0$ ms), the pressure is zero in the complete tentacle. Thus, the tentacle is assumed to be initially 'stress free' and any gravity effects are neglected. To obtain a satisfactory resolution of the pressure gradient at each selected instant, all segmental pressures were normalized with respect to the instantaneous maximum in the stalk. Colours from the scale in figure 8 were assigned to these normalized pressures. Immediately after the start, force development in the extensor muscles sets up a negative pressure gradient in the tentacular stalk from
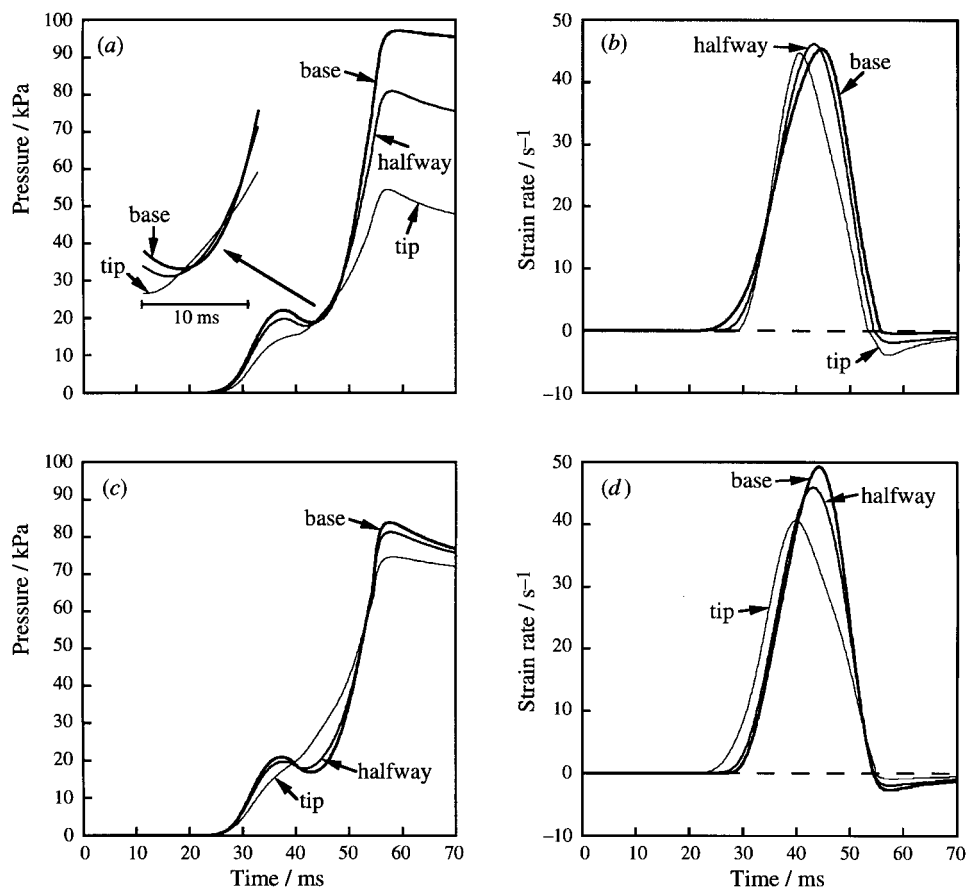
Figure 9. (*a*) Pressure variation at the tentacular base (bold curve), halfway along the tentacular stalk (normal), and tip of the stalk (thin) for the extension of figures 7 and 8 with optimized myosin filament lengths. (*b*) Longitudinal strain rate at the tentacular base (bold curve), halfway along the tentacular stalk (normal), and tip of the stalk (thin) for the extension of figure 7 and 8. A portion of the plot is expanded at the inset. (*c*) Pressure variation at the tentacular base (bold curve), halfway along the tentacular stalk (normal), and tip of the stalk (thin) for an extension similar to figure 7 and 8, but with the same myofilament lengths along the stalk. (*d*) Like (*c*), but now for the longitudinal strain rates ($l_{myo} = 0.7352\,\mu m$).

base to tip (recall that we do not consider the pressure gradient in the club). Tentacular segments are accelerated forward because of this gradient. The frames at 42.5, 45 and 47.5 ms indicate that the pressure is very similar over the complete tentacular stalk. The resolution of the colour gradient (10% of the maximum pressure) is insufficient to show details of the pressure gradient for these frames. Figure 9*a* shows pressure curves for the base and the tip of the stalk and a position halfway along stalk, indicating that in this phase of the strike (42.5–47.5 ms) the pressure gradient is temporarily even very slightly reversed. This change in the pressure gradient corresponds fairly closely to the sign reversal of the acceleration of the tentacular club (figure 7*e*). Deceleration in this phase and the following phase, however, is mainly due to the viscous and elastic effects.

Figure 9*b* shows the longitudinal strain rates for the three positions along the stalk. The extension rate is initially highest at the base of the stalk. The most distal stalk segment is even very slightly compressed. From about 35 ms, the gradient in the extension rate reverses. Highest longitudinal strain rates are found at the tip of the stalk from about 35–41 ms. The longitudinal strain rates at the base and the tip

are both fairly high when the strain rate half way along the stalk reaches its peak, resulting in a good overall peak performance. The subsequent drop in the strain rate occurs first distally and last at the most proximal position.

(*c*) *Effect of myofilament lengths on extension performance*

In the previous subsection, we have used the optimized filament lengths. Let us now compare the pressures and strain rates for a tentacular design with constant filament lengths in the extensor muscles along the complete stalk (figure 9*c, d*). The average lengths of the optimized case were applied for this purpose (i.e. $l_{myo} = 0.7352\,\mu m$). Figure 9*c* shows that (compared to the optimized case) the initial pressure difference between base and tip is smaller, and the (unfortunate) reversal of the pressure gradient occurs earlier and lasts longer, which would tend to decrease the forward acceleration. Figure 9*d* shows that the peak strain rate in the distal segment has dropped considerably compared to the optimized situation of figure 9*b*. The sarcomeres in this range are too slow for the relatively low mechanical load. The distal lon-
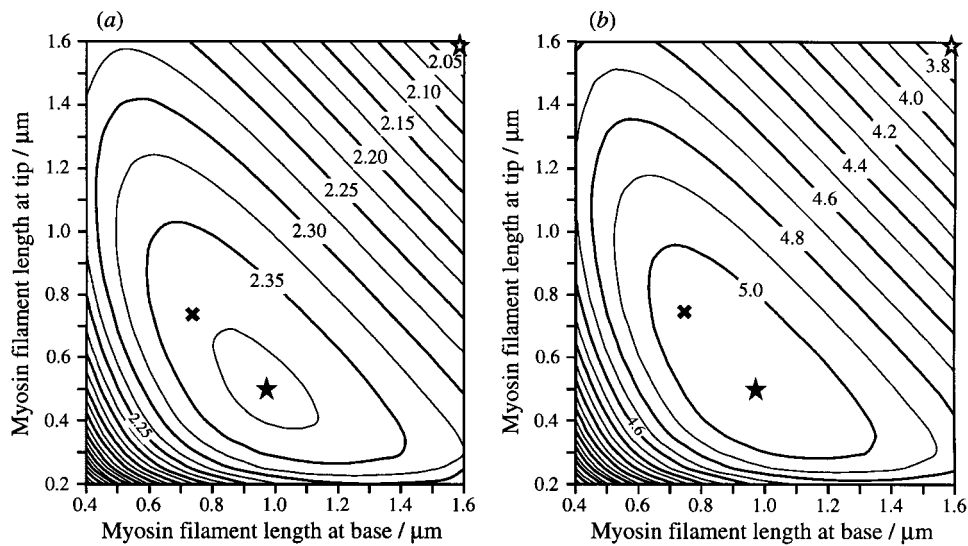
Figure 10. (*a*) Contour plot illustrating the effect of the variation of the proximal and distal thick filament lengths on the peak velocity of the terminal club. Peak velocities in m s^{-1} are given next to contours. (*b*) Contour plot showing the effect of the variation of the proximal and distal thick filament lengths on the peak kinetic energy of the terminal club. Energy values of contours are in mJ. To save computational time, contour calculations were performed with 26 segments. Specific points were calculated with 51 segments. Filled star, global maximum; open star, predicted performance for vertebrate sarcomere design.

gitudinal strain rate in the stalk has dropped considerably at the moment that the peak rate occurs half way along the stalk. In comparison with the optimized case, these phenomena correspond to a slightly lower overall peak extension rate of the stalk.

The contour plot of figure 10*a* shows the effect of myosin filament length along the stalk on the peak extension velocity. The myosin filaments at the base and the tip of the stalk were varied and the intermediate lengths were linearly interpolated. Basically, the contour plot shows a curved ridge on top of which the peak extension velocity varies only moderately. At right angles to this ridge, the velocity drops much more quickly. The global velocity maximum of 2.3772 m s^{-1} (calculated with $n = 51$, located at the black star in figure 10*a*) is obtained with $l_{\mathrm{myo},1} = 0.9707\,\mu$m at the base and $l_{\mathrm{myo},50} = 0.4997\,\mu$m at the tip.

The black cross in figure 10*a* indicates the performance with equal filament lengths along the stalk (value identical to those of figure 9*c*, *d*; $l_{\mathrm{myo}} = 0.7352\,\mu$m). The peak velocity is still approximately 99% of the global maximum. Thus, the performance is not dramatically decreased if the filament lengths are fairly close to the absolute optimum values. Taking values, however, that are significantly shorter or longer results in a dramatic decrease in performance (especially lower-left and upper-right corners of figure 10*a*). In this respect, it is interesting to explore what the performance would be of a typical vertebrate sarcomere (keeping the maximum interfilamentary velocity constant). The thick filament length in vertebrates is approximately 1.58 μm (Offer 1987), and remarkably invariant (see also §7). The vertebrate design is represented by the open star in the upper-right corner of figure 10*a*. For the vertebrate

design, the peak velocity of the terminal club is predicted to be only about 85% of the global optimum. The myofilament lengths of the vertebrate sarcomere would be too long for the remarkably low local mechanical load in the tentacle, i.e. the generated interfilamentary sliding speeds would be (for a considerable period of the strike) much too high for an optimal power output. Thus, a vertebrate sarcomere geometry would be considerably less effective than the actual sarcomere geometry.

A significant drop in the peak velocity results if the myosin filament length at the tip is longer than the value at the base. This can be understood as follows. The most distal segments of the stalk have in front of them the lowest mass to be accelerated. Placing the longest filaments in this area leads to considerable (initial) local pressures which can even exceed the proximal pressures. This leads to an overloading of the proximal segments which initially shorten and widen, and therefore produce negative work. Thus, the proximal parts take up energy that is liberated in the distal segments. This reduces the peak velocity of the club. This unfortunate effect may be slightly compensated for by storage of some of the absorbed energy as strain energy. In addition, prestretched muscle fibres may produce somewhat higher tensile stresses during subsequent shortening.

In conclusion, negative local power output should be avoided or very much limited. In comparison, a very small amount of negative muscle work may be produced in the most posterior myotomes of some fish, such as carp, swimming in a cyclical mode (e.g. Van Leeuwen *et al.* 1990; Van Leeuwen 1995). Here, muscle tissue can regulate the stiffness of the caudal peduncle and therefore the force transmission from rostral myotomes to the caudal fin. For fish with a range of swimming styles, this may lead to a better

overall hydrodynamic efficiency. Such an option is, however, not available for the tentacle.

We found that the optimum values of the myofilament lengths are sensitive to the nature of the longitudinal elastic counter forces and the maximum unloaded interfilamentary velocity. This does not influence the general conclusion that remarkably short (and decreasing) myofilament lengths from base to tip are advantageous (with zero tapering of the stalk and identical cross-bridge dynamics), but very exact predictions of optimal filament lengths are only possible if more detailed data become available of various tissue mechanical properties. We have used a fairly high value for the maximum unloaded interfilamentary sliding velocity. Therefore, we have probably not underestimated the optimal length of the myofilaments (a higher unloaded interfilamentary sliding velocity leads to longer optimal filament lengths).

Figure 10*b* shows the effect of the length of the myosin filament length on the peak kinetic energy of the tentacular club. This plot is simply obtained by taking the square of the velocities in figure 10*a* and multiplication by half the club mass. Naturally, this leads to a greater sensitivity to changes in myofilament lengths, but not to a shift in the maximum. The global maximum (filled star) is about 5.08 mJ. It is predicted that with the vertebrate sarcomere design (open star) only about 73% of the global maximum could be generated.

We conclude that an adjustment of myofilament lengths along the stalk is beneficial for maximization of the peak velocity and peak kinetic energy of the stalk and club. Such an adjustment is expected to increase the efficacy of prey capture. In this way, sarcomere ultrastructure can be linked to the gross morphological dynamics of the tentacular system.

7. GENERAL DISCUSSION

The model is capable of reproducing fairly accurately the tentacle extension in *Loligo pealei*. To achieve this performance, we had to estimate several parameters for which no independent measurements were available. We had no other choice than following this procedure, since measurement of every parameter would take several years. Nevertheless, none of the estimated parameter values was out of the range of generally accepted values for vertebrate and invertebrate muscle fibres. Thus, the seemingly exceptional performance is probably achieved with typical muscle characteristics. The rise time chosen for the activation in the extensor muscles is quite short and the maximum unloaded interfilamentary velocity is quite high. It should, however, be expected that these parameters have been optimized in squid tentacles because a good extension performance has a great survival value. Indeed, Kier (1985, 1991) has described a remarkably well-developed sarcoplasmic reticulum, suggesting a rapid activation capability. The maximum interfilamentary velocity has yet to be measured.

Our simulations suggest that use of previously stored elastic energy does not seem to be required for the observed extension performance. Nevertheless, liberation of elastic energy during the strike cannot be completely excluded given the lack of experimental data. It could be possible that initially a coactivation of the longitudinal muscles and the extensor muscles occurs. This would, however, require a very rapid deactivation of the longitudinal muscles. Such a coactivation is absent in the tongue of the chameleon (Wainwright & Bennett 1992*a*). Future electromyographic recordings may help to resolve these uncertainties about the tentacle.

The model assumes a constant value for the fluid pressure in each compartment, thus prohibiting a pressure gradient in the transverse direction. Furthermore, the model does not allow the muscle fibres to curve, whereas curved fibres under tension influence the pressure gradient in muscle tissue (Van Leeuwen & Spoor 1992, 1993). It may, however, be argued that a well-balanced mechanical design would actually minimize the muscle fibre curvature along the stalk. Presently, a more complex model is under development which takes both aspects into account and which includes also the longitudinally and the helically arranged muscle fibres.

The extension velocity of the tentacle can be optimized by adjustment of several factors. Examples are the: (1) adjustment of the tentacular shape (change) for a low water resistance; (2) adjustments of the muscle architecture (i.e. geometrical arrangement of the muscle fibres); (3) adjustments in the geometrical properties of the sarcomeres; (4) adjustments in the properties of the enzymes involved in the contraction process; (5) optimization of the timing of the activation along the tentacle; and (6) the risetime of the activation. Although we have concentrated here on the sarcomere geometry, it should be recognized that these parameters interact strongly. For instance, an increase in the rate of the contractile processes at the cross-bridge level would shift the optimum myofilament lengths to greater values.

Data from the literature (Kier 1985, 1991) show that the myofilament lengths are remarkably short and quite variable in the extensor muscles (0.5–0.9 μm). Myofilament lengths as a function of the position along the tentacle have still to be measured. The present model shows indeed that short myofilament lengths are required for an optimal peak extension velocity (given that enzymatic variations and tapering of the stalk are relatively unimportant), and that the optimum length should vary considerably along the tentacular stalk. It would be of great interest to investigate the cellular control mechanism of myofilament lengths, if squid do indeed adjust the sarcomere geometry to the local mechanical load.

The myofilament lengths in the longitudinally and helically arranged muscle fibres are very long (myosin filament length is about 6.0 μm). This allows relatively high contraction forces to be generated with a small cross-sectional area. The resulting small mass of these two muscle fibre groups is advantageous for the extension performance. These obliquely striated

muscles probably have very long actin filaments in comparison with the myosin filament length. This provides a means of generating a relatively large force over the wide range of strain experienced by these fibres.

It may be surprising that in vertebrate cross-striated muscles the myosin filament length is fairly constant. Here, however, the required local tissue loading can be easily adjusted by a combination of changes in muscle architecture and moment arms of the muscles about their joints, whereas in the squid tentacle a transverse arrangement of the extensor muscles is obviously optimal for an optimization of the extension velocity. Thus, for an optimal performance, fibre directions of the extensor muscles should be limited to transverse planes. A further optimization is achieved by geometric adjustments at the sarcomere level; the low mechanical load requires very short sarcomeres for an optimal performance. Very short sarcomeres, however, are fairly costly because of the relatively high number of required Z-discs and bare zones on the myosin filaments. It therefore may not be surprising that vertebrate skeletal muscles have longer sarcomeres than those of tentacular extensor muscles.

Why are vertebrate myosin filaments not longer than they are? This question is not easy to answer. The strength of the Z-disc or actin filaments may for instance be limiting. In insects, longer myosin filaments are found in cross-striated muscles, but here more actin filaments are present per myosin filament.

Vertebrates that use rapid tongue extensions for prey capture like chameleons (e.g. Wainwright *et al.* 1991), plethodontid salamanders (e.g. Lombard & Wake 1977) and frogs (e.g. Gans & Gorniac 1982) have to our knowledge not evolved very short sarcomeres. In contrast, these animals have developed adaptations for relatively strong kinematic transmissions at the gross morphological level. In frogs, this can for instance be achieved by a rapid straightening of a previously curved tongue. While such a mechanism can be successfully applied in air, in water it would fail completely due to the high drag of the water. In the chameleon, however, the projected tongue follows an almost straight path. Here, the tongue slides over the entoglossal bone, which is a slender rod with a tapered distal end (Wainwright & Bennett 1992*a*, *b*). The main accelerator muscle has muscle fibres that run in complex curves from the central muscle boundary to the periphery (again optimally oriented in transverse planes, cf. Van Leeuwen (1997)). The muscle is wrapped around the entoglossal bone. Our present model can be adapted for a description of the tongue projection in the chameleon. From a preliminary analysis, we conclude that, compared to the squid tentacle, a higher extension rate can be generated for a given strain rate in the extensor muscles. The higher extension rate is caused by the sliding movement of the accelerator muscle over the tapering end of the entoglossal bone. Thus, we expect the optimal sarcomere length in the chameleon to be longer than in the squid. Figure 5*b*, based on equation (25), shows that the longitudinal strain rate increases with

tentacle length for a given (negative) muscle strain rate. This change in kinematic transmission (gearing) is favourable since it allows the muscle fibres to remain closer to the optimum power output (figure 4*b*) at the highest extension rates generated. Our preliminary calculations suggest that an even more effective change in the kinematic transmission is present in the tongue of the chameleon.

Why are squid tentacles so thin? Further research is required to address this issue in a detailed quantitative manner. We wish to make, however, the following suggestions. First, in the modelling section, we have shown that an addition of muscle tissue in the radial direction has only a very limited effect on the extension speed, in contrast to an addition in the longitudinal direction. The tentacle should, however, be thick enough to avoid substantial buckling. In *Loligo pealei*, two arms are used to stabilize the thin tentacles during extension (Kier & Van Leeuwen 1997). Second, the elongated shape leads to a very low effective added mass of water and a minimal disturbance of the flow field around the prey before the clubs attach to the prey. Although the clubs are slightly larger in diameter than the stalk, they are elongate and also have a low added mass. The size of club is an important determinant of the dynamic loading of the stalk. Third, the prey probably receives a relatively small visual stimulus from a thin tentacle.

In the modelling section, we have suggested that the local driving extension force that can be exerted is proportional to the local cross-sectional area A_c. In isometric growth, A_c is proportional to l^2 (l is any length measure), but the mass to be pushed forward is proportional to l^3. Thus, the relative load increases with l. We therefore expect to see a drop in the acceleration capabilities and an increase in the extension time with isometric growth if the sarcomere properties remain constant. Purely isometric growth, however, is unlikely to occur. It would be interesting to investigate whether allometric growth is such that extension performance is maximized for each size. The acceleration drop with size may be partially compensated by increasing the myofilament lengths during growth. Additionally, large squid will tend to capture large prey with lower acceleration capabilities than smaller prey. The unavoidable increase in extension time with growth may nevertheless set a limit to the size above which tentacles can no longer be used to capture rapid prey. We hope that the model proposed here will be a useful tool in future scaling studies.

The present model reveals several gaps in the knowledge of the tissue properties of the squid tentacle, while many more predictions can be made than can presently be tested. For instance, we need more data on: (1) myo-filament lengths along the tentacular stalk; (2) force–length, force–velocity and activation characteristics of the muscle fibres; (3) the actual activation along the stalk of the muscle fibres of the various muscle groups; (4) local variations of the strain and intramuscular pressure during the strike; and (5) tentacle growth. In this respect, we hope that

our model will be helpful in directing future morphological and physiological observations. Our understanding of squid tentacles would be significantly improved by an integrated quantitative model of: (1) the dynamics of the muscular system; (2) the dynamics of the nervous system that controls it; and (3) the mechanics of the external fluid flow.

8. CONCLUSIONS

(1) In the forward dynamics model proposed here, the extension of the tentacles in squid is calculated from morphological and physiological properties of the tentacular tissue, and an assumed activation of the sarcomeres of the extensor muscles. The model is capable of reproducing fairly accurately the observed tentacle extension in *Loligo pealei*.

(2) The kinematic analysis by Kier & Van Leeuwen (1997) has shown that a remarkable performance is achieved in the tentacle extension movement by squid. The model predicts that this performance can be realized with physiological properties of the extensor muscles fibres that are in the range of previously investigated striated muscle cells. It is proposed that the high longitudinal strain rate results from a combination of a short rise time of the activation of the extensor muscles, a fairly high maximum interfilamentary sliding velocity, very short myofilament lengths and the arrangement of the extensor muscle fibres at right angles to the long axis in an almost incompressible fluid environment. Thus, a loading of the microactuators (i.e. the cross-bridges) in the muscular system that is optimal for a high peak extension velocity can be achieved by a combination of ultrastructural and gross morphological adaptations. A rapid release of elastic energy does not seem to be required for the extension movement, but cannot presently be completely excluded.

(3) In spite of the very short myofilament lengths (resulting in fairly low tensile stresses), the intramuscular pressures in the system are probably fairly high (approximately 20 kPa during the acceleration phase, about the same magnitude as the measured and expected pressures in vertebrate skeletal muscles (Van Leeuwen & Spoor 1992 and references therein). This results from the transverse orientation (at right angles to the circumferential surface) of the bulk of the extensor muscles. The generation of a strongly negative pressure gradient from base to tip along the tentacular stalk results in the rapid forward acceleration of tentacular tissue.

(4) To achieve the highest possible peak extension velocity, muscle fibre properties should vary throughout the tentacular stalk. The present model predicts an optimal myosin filament length of about $0.97\,\mu\text{m}$ at the base of the tentacular stalk and about $0.5\,\mu\text{m}$ at the tip of the stalk. In this analysis, it is assumed that the enzymes associated with the actin–myosin interaction do not vary along the stalk. The predicted range agrees with the range of reported thick filament lengths (Kier 1985, 1991). Observations of myosin filament lengths and enzymatic profiles along the stalk

are needed to test the assumptions and predictions of the model. In addition, future work is planned to address effects of scale on the design of the tentacles.

APPENDIX 1. ADDITIONAL FORMULAE

Here, we will derive expressions for the components c in equation (45). Let us first make the following definitions:

$$g_{1,i} = -\dot{h}_i \dot{r}_i/(2h_i), \qquad (48)$$

$$g_{2,i} = \dot{h}_i^2 r_i/(2h_i^2), \qquad (49)$$

$$g_{3,i} = -r_i/(2h_i), \qquad (50)$$

$$g_{4,i} = \eta \sigma_{r,i} A_{s0,i}/A_{s,i}, \qquad (51)$$

$$g_{5,i} = m_i(\tfrac{1}{2} + \alpha)/A_{s,i}, \qquad (52)$$

$$g_{6,i} = -\sigma_{l,i} A_{cl0} - \dot{\varepsilon}_{l,i}\mu A_{cl0}. \qquad (53)$$

By substitution, equations (33), (38), and (42) can now be written as

$$\ddot{r}_i = g_{1,i} + g_{2,i} + g_{3,i}(a_i - a_{i-1}), \qquad (54)$$

$$p_i = g_{4,i} + g_{5,i}\ddot{r}_i, \qquad (55)$$

$$F_i = p_i A_{c,i} + g_{6,i}. \qquad (56)$$

By subsequent substitution of (54) into (54), (54) into (54), and (54) into (44), the following equation is obtained:

$$a_{i-1}c_{1,i} + a_i c_{2,i} + a_{i+1}c_{3,i} = c_{4,i}, \qquad (57)$$

where

$$c_{1,i} = \frac{g_{3,i}g_{5,i}A_{c,i}}{m_{b,i}}, \qquad (58)$$

$$c_{2,i} = 1 - \frac{g_{3,i}g_{5,i}A_{c,i} + g_{3,i+1}g_{5,i+1}A_{c,i+1}}{m_{b,i}}, \qquad (59)$$

$$c_{3,i} = \frac{g_{3,i+1}g_{5,i+1}A_{c,i+1}}{m_{b,i}}, \qquad (60)$$

$$c_{4,i} = \frac{(g_{4,i} + g_{5,i}(g_{1,i} + g_{2,i}))A_{c,i}}{m_{b,i}}$$
$$- \frac{(g_{4,i+1} + g_{5,i+1}(g_{1,i+1} + g_{2,i+1}))A_{c,i+1}}{m_{b,i}}$$
$$+ \frac{g_{6,i} - g_{6,i+1}}{m_{b,i}}. \qquad (61)$$

All the c components in (45) can now be calculated from these equations by substituting appropriate values for i, while taking into account the boundary conditions at the base and the tip of the stalk as defined in §5.

REFERENCES

Abbott, B. C. & Baskin, R. J. 1962 Volume changes in frog muscle during contraction. *J. Physiol.* **161**, 379–391.

Aubert, X. 1956 Le couplage énergétique de la contraction musculaire. Thesis, Editions Arscia, Brussels.

Gans, C. & Gorniac, G. C. 1982 How does the toad flip its tongue? Test of two hypotheses. *Science* **216**, 1335–1337.

Gordon, A. M., Huxley, A. F. & Julian, F. J. 1966 The variation in isometric tension with sarcomere length in vertebrate muscle fibres. *J. Physiol.* **184**, 170–192.

Guérin, J. 1908 Contribution à l'étude des systèmes cutané, musculaire et nerveux de l'appareil tentaculaire des Céphalopodes. *Arch. Zool. Exp. Gén.* (série 4) **8**, 1–178.

Hill, A. V. 1938 The heat of shortening and the dynamic constants of muscle. *Proc. R. Soc. Lond.* B **126**, 136–195.

Huxley, A. F. & Niedergerke, R. 1954 Structural changes in muscle during contraction. Interference microscopy of living muscle fibres. *Nature* **173**, 971–973.

Josephson, R. K. 1975 Extensive and intensive factors determining the performance of striated muscle. *J. Exp. Zool.* **194**, 135–154.

Kier, W. M. 1982 The functional morphology of the musculature of squid (Loliginidae) arms and tentacles. *J. Morphol.* **172**, 179–192.

Kier, W. M. 1985 The musculature of squid arms and tentacles: ultrastructural evidence for functional differences. *J. Morphol.* **185**, 223–239.

Kier, W. M. 1991 Squid cross-striated muscle: the evolution of a specialized muscle fibre type. *Bull. Mar. Sci.* **49**, 389–403.

Kier, W. M. & Schachat, F. H. 1992 Biochemical comparison of fast and slow contracting squid muscle. *J. Exp. Biol.* **168**, 41–56.

Kier, W. M. & Smith, K. K. 1985 Tongues, tentacles and trunks: the biomechanics of movement in muscular-hydrostats. *Zool. J. Linnean Soc.* **83**, 307–324.

Kier, W. M. & Van Leeuwen, J. L. 1997 A kinematic analysis of tentacle extension in the squid *Loligo pealei. J. Exp. Biol.* **200**, 41–53.

Lighthill, J. 1986 *An informal introduction to theoretical fluid mechanics.* Oxford University Press.

Lombard, R. E. & Wake, D. B. 1977 Tongue evolution in the lungless salamanders, Family Plethodontidae. II. Function and evolutionary diversity. *J. Morph.* **153**, 39–80.

Messenger, J. B. 1968 The visual attack of the cuttlefish, *Sepia officinalis. Anim. Behav.* **16**, 342–357.

Messenger, J. B. 1977 Prey capture and learning in the cuttlefish, *Sepia. Symp. Zool. Soc. Lond.* **38**, 347–376.

Nelder, J. A. & Mead, R. 1965 A simplex method for function minimization. *Comp. J.* **7**, 308–313.

Offer, G. 1987 Myosin filaments. In *Fibrous protein structure* (ed. J. M. Squire & P. J. Vibert), pp. 307–356. London: Academic Press.

Otten, E. 1987 A myocybernetic model of the jaw system of the rat. *J. Neurosci. Meth.* **21**, 287–302.

Press, W. H., Flannery, B. P., Teukolsky, S. A. & Vetterling, W. T. 1989 *Numerical recipes in Pascal. The art of scientific computing.* Cambridge University Press.

Van Leeuwen, J. L. 1991 Optimum power output and structural design of sarcomeres. *J. Theor. Biol.* **149**, 229–256.

Van Leeuwen, J. L. 1992 Muscle function in locomotion. In *Mechanics of animal locomotion* (ed. R. McN. Alexander). Advances in comparative and environmental physiology 11, pp. 191–250. Heidelberg: Springer.

Van Leeuwen, J. L. 1995 Review article: The action of muscles in swimming fish. *Exp. Physiol.* **80**, 177–191.

Van Leeuwen, J. L. 1997 Why the chameleon has spiral-shaped muscle fibres in its tongue. *Phil. Trans. R. Soc. Lond.* B **352**, 573–589. (Following paper.)

Van Leeuwen, J. L., Lankheet, M. J. M., Akster, H. A. & Osse, J. W. M. 1990 Function of red axial muscles of carp (*Cyprinus carpio*): recruitment and normalized power output during swimming in different modes. *J. Zool. Lond.* **220**, 123–145.

Van Leeuwen, J. L. & Spoor, C. W. 1992 Modelling mechanically stable muscle architectures. *Phil. Trans. R. Soc. Lond.* B **336**, 275–292.

Van Leeuwen, J. L. & Spoor, C. W. 1993 Modelling the pressure and force equilibrium in unipennate muscles with in-line tendons. *Phil. Trans. R. Soc. Lond.* B **342**, 321–333.

Wainwright, P. C. & Bennett, A. F. 1992*a* The mechanism of tongue projection in chameleons. I. Electromyographic tests of functional hypotheses. *J. Exp. Biol.* **168**, 1–21.

Wainwright, P. C. & Bennett, A. F. 1992*b* The mechanism of tongue projection in chameleons. II. Role of shape change in a muscular hydrostat *J. Exp. Biol.* **168**, 23–40.

Wainwright, P. C., Kraklau, D. M. & Bennett, A. F. 1991 Kinematics of tongue projection in *Chameleo oustaleti. J. Exp. Biol.* **159**, 109–133.

Williams, L. W. 1909 *The anatomy of the common squid* Loligo pealii, *LeSueur.* Leiden: E. J. Brill.

Woledge, R. C., Curtin, N. A. & Homsher, E. 1985 *Energetic aspects of muscle contraction.* Monographs of the Physiological Society, no. 41. London: Academic Press.

Woltring, H. J. 1986 A Fortran package for generalized, cross-validatory spline smoothing and differentiation. *Adv. Engng Software* **8**, 104–113.